POLARIZATION SENSITIVITY OF MONOPULSE RADAR BORESIGHT ERROR INDUCED BY LARGE, OGIVE RADOMES

THESIS

Kelce S. Wilson
Captain, USAF

AFIT/GE/ENG/94D-31

DEPARTMENT OF THE AIR FORCE
AIR UNIVERSITY
AIR FORCE INSTITUTE OF TECHNOLOGY

Wright-Patterson Air Force Base, Ohio

AFIT/GE/ENG/94D-31

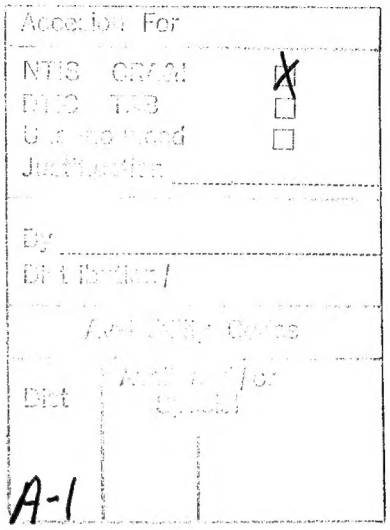

POLARIZATION SENSITIVITY OF MONOPULSE RADAR BORESIGHT ERROR INDUCED BY LARGE, OGIVE RADOMES

THESIS

Kelce S. Wilson
Captain, USAF

AFIT/GE/ENG/94D-31

Approved for public release; distribution unlimited

AFIT/GE/ENG/94D-31

POLARIZATION SENSITIVITY OF MONOPULSE RADAR BORESIGHT ERROR INDUCED BY LARGE, OGIVE RADOMES

THESIS

Presented to the Faculty of the School of Engineering

of the Air Force Institute of Technology

Air University

In Partial Fulfillment of the

Requirements for the degree of

Master of Science in Electrical Engineering

Kelce S. Wilson, B.S.E.E.

Captain, USAF

December 1994

Acknowledgements

I'd like to thank Captain Mike Temple, for his patient and extensive help. His assistance from the very start of the research through editing this thesis was invaluable. I'd also like to thank my advisor, Dr. Vittal Pyati, for giving me such an excellent topic and his inputs for improving the write-up.

I would like to thank my wife, Robyn, and my daughter, Kalyn, for their understanding and sacrifice while I was so busy with AFIT. Thank you also to my committee members, Captain Paul Skinner, who was kind enough to re-derive the equations, and Major Gerace, who was readily available for questions and advice.

Finally, I would like to thank my sponsoring organization, WL/AAWD-1, for the use of their equipment and allowing Captain Temple to spend so much time with me.

Table of Contents

List of Figures

POLARIZATION SENSITIVITY OF MONOPULSE RADAR BORESIGHT ERROR INDUCED BY LARGE, OGIVE RADOMES

1. Introduction

Boresight Error (BSE) is defined as the angular difference between a target's actual and radar-indicated position and is influenced by the radome used to protect the antenna from the elements and for streamlining purposes. A reliable computer modeling technique for predicting the BSE of electrically large radar-radome systems has been demonstrated [1]. This modeling technique, based on a ray-trace receive formulation using Geometric Optics (GO), was extended in this effort by investigating the dependence and sensitivity of radome-induced BSE for various combinations of scan angle, element polarization, and incident Electric Field (E-Field) polarization. Results obtained compare very well with empirical, published, and experimentally measured data for specific scan angle and polarization cases considered. Generally, BSE exhibits a noticeable dependence on reference E-Field polarization, except under limited scanning conditions for specific Linear Polarization (LP) cases.

1.1 Background

Monopulse processing systems can precisely locate targets using a single pulse of Radio Frequency (RF) energy. Because of their accuracy and speed, monopulse

techniques are used extensively in modern military aircraft fire control radars and missile seeker/guidance systems [2]. One of the important performance metrics of such radar systems consists of analyzing BSE under varying conditions of aperture scan angle, element polarization, incident E-Field polarization, and radome geometry. A pictorial depiction of BSE is shown in Chapter 2, Figure 1.

An ideal radome would be entirely transparent across the electromagnetic (EM) spectrum of interest. This implies no amplitude, phase, or polarization distortions introduced to any EM wave passing through it. However, production constraints and available radome materials necessitate compromises between EM transparency, aerodynamic performance, and structural integrity. A practical radome is far from ideal for EM wave propagation. There are bound to be refractive and reflective distortions at the radome material boundaries. These distortions are a major source of BSE.

Distortional effects are further complicated by aperture scanning within the radome, either electronically or mechanically, in both horizontal and vertical directions to track targets at arbitrary aspect angles. As a result, radar waves intercept the radome at varying angles and illuminate different portions of the radome walls. Hence, wavefront distortion, and therefore BSE, becomes a function of aperture scan angle.

Recent results have shown that monopulse BSE can be accurately predicted with GO-based computer algorithms for electrically large radar-radome systems. This effort builds on previous research efforts [1,3,4,5] which successfully characterized BSE for systems using tangent ogive radomes. Generally, past efforts have focused on the scan angle dependence of system BSE for a limited number of polarization cases and identified scan regions which inherently possess greater BSE degradation. This effort extends these

results by performing an analysis which is primarily driven by polarization sensitivity effects. A previously developed/validated modeling technique [1] served as the basis for the current work because of its adaptability to polarization variations. Specifically, the technique was developed for arbitrarily located and polarized reference E-Fields and arbitrarily orientated and polarized aperture elements.

1.2 Problem Statement

Ability to predict system BSE prior to actual radar and radome construction allows one to optimize/minimize BSE without incurring the large fabrication costs of multiple prototypes. If alternate radar-radome system designs can be analyzed for best-case BSE using computer model results, a design may be chosen without an iterative build and test process. The use of Circular Polarization (CP) radar apertures raises the question of whether BSE remains constant over all possible received E-Field polarization states, since CP elements have the desirable feature of being able to intercept an incident field of arbitrary polarization. This effort seeks to validate a computer modeling technique for use in optimizing radome design in terms of BSE polarization sensitivity.

A common method of accounting for radome-induced BSE is to use a look-up table calibrated for the specific radar-radome combination, which provides an error-correction factor in a given scan direction. Since BSE may vary with reference E-Field polarization, it may become multi-valued for a single scan direction, if the polarization of an incident E-Field varies. One may then require a multi-dimensional look-up table

(azimuth, elevation, and incident field polarization versus BSE) instead of the presently used two-dimensional table (angle off-boresight versus BSE).

Many factors can introduce a degree of randomness into the polarization of a received radar wave and cause it to differ from the transmitted wave; atmospheric effects can alter the orientation of the E-Field, enemy jammers can be arbitrarily polarized, and target geometry can cause reflected energy to be differently polarized than the incident energy. For example, a target composed of flat plates and sharp edges, all nearly parallel to or contained in a single plane, will reflect predominantly LP aligned with the edges. In such a case, an RCP or LCP transmitted radar wave would be reflected and returned as elliptically polarized, with a predominant LP component. The tilt angle of the returned LP component would be determined by the flight attitude of the target, and therefore would be entirely random to the radar receiver. This randomness will generally introduce uncertainty in the actual BSE.

Apertures using LP elements expect to receive reflected energy of nearly identical polarization as the transmitted energy. Although atmospheric effects, radome effects, and target geometry will change the orientation of the E-Field, the energy returned from the target will remain predominantly aligned with the aperture elements.

1.3 Summary of Current Knowledge

Two prior research efforts formed the basis for this investigation. By far, the most important was a recent PhD dissertation by Captain Michael Temple, USAF, while at the Air Force Institute of Technology. This dissertation work provided the basic computer

modeling technique, which, with minor modifications, provided the data given in Chapter 4. The basic computer model and subsequent modifications are described in Chapter 3.

Temple showed [1,6] that a GO-based computer algorithm could accurately predict the BSE of a production radar/radome system. The model was written to accommodate arbitrary reference E-Field polarization and aperture specifications, including the number, locations, weightings, phases, polarizations, and field patterns of the elements. When applied to an actual production system, model BSE prediction results were within 1.0 milliRadian (mRad) of measured data. Flexibility, speed, and adaptability to modifications made Temple's model particularly suitable for this research effort.

David G. Burks was one of the first investigators to predict BSE for multiple polarization cases using GO computer modeling techniques [2]. Burks characterized BSE as a function of scan angle for each of six different polarization cases. The six cases included RCP and five LP states of various tilt angle. These BSE results are distinctly different for each of the polarization cases, and clearly indicated that BSE is generally a function of both scan angle and reference E-Field polarization.

Other publications were found relating to radome-induced BSE, however, most used surface integration of equivalent currents on the radome, rather than GO, or were limited to a single polarization. Surface integration is more computationaly intensive than the GO method, and so is generally not practical for electrically large radomes.

1.4 Assumptions and Scope

Several assumptions and approximations are essential to assure computational efficiency. The assumptions and approximations used in this effort are consistent with

those used by Temple, who computed the half-power beamwidth (HPBW) of a production aperture within 0.5% of the production specification, and the gain within 0.1 dB [1:133]. The scope of the problem addressed is restricted by the conditions under which the approximations hold and by limiting the number of radar-radome combinations analyzed.

Although the radome surface is curved, locally planar approximations are used at each point that an E-Field ray intersects the surface boundary. This allows the use of transmission and reflection coefficients for a plane wave incident on a homogenous dielectric half-space, i.e., Fresnel coefficients.

The radar antenna is modeled as a quadrant symmetric aperture with an identical field pattern and polarization response for each element. For any given array, mutual coupling between aperture elements affects the individual responses. An element near the center of the array is surrounded by many "neighboring" elements, while an edge element has fewer "neighbors". Therefore, mutual coupling effects are generally different for center and edge elements. For large, densely populated arrays, the elements near the center significantly outnumber the edge elements. Since mutual coupling effects are primarily due to the relatively few "nearer-neighbor" elements, the effects will be similar for the majority of the elements. Also, most practical apertures use a tapered amplitude weighting, further reduced the effect of mutual coupling differences.

The evaluation of electrically large radar-radome systems, a minimum of 5λ to 28λ wide by 14λ to 90λ long, allows the use of a GO-based analysis, which is more computationaly efficient than a surface integration method for the geometry sizes used.

This analysis addresses single layer ogive radome designs with roughly a 3-to-1 length to width ratio (fineness ratio). An exception from this shape is a hemispheric

radome used for model validation. The aperture is limited to LP, RCP, and LCP elements with a cosine field pattern response to co-polarized E-Fields. LP elements have a fixed tilt angle and a -20 dB cosine field pattern response to cross-polarized E-Fields. The polarization of cross-polarized E-Fields is orthogonal in the aperture plane to the element polarization.

Variations in the reference E-Field polarization are primarily limited to LP fields with tilt angles varying between ±90°, referenced to an arbitrarily oriented vector. Tilt angles outside this range are redundant; they can be represented by tilt angles within the range by applying a 180° phase shift to the field strength, allowing all possible linear polarizations to be referenced against the same arbitrary vector. Using redundant tilt angles would not provide different BSE values or any more insight (except for a few cases used to validate the model). Several cases were run with elliptically polarized incident waves, including both RCP and LCP. For these cases, BSE variations due to polarization changes were muted in comparison with the LP cases. The plotted results are exclusively of BSE versus tilt angle of LP reference E-Fields.

1.5 Thesis Overview

Analysis and modeling results, generated on a MICROVAX processing system using a standard Fortran language, are validated against previously published data [1,3] and contractor furnished data on a production radome-radar system. Predicted BSE was within 1.0 mRad of published and production data for all polarization cases considered. Previously validated cases are extended by predicting BSE sensitivity effects under

numerous polarization states, i.e., various linear/circular combinations of aperture element and reference E-Field polarization. Analysis and modeling results clearly indicate that 1) given LP aperture elements, radome-induced BSE is dependent on both aperture scan angle and reference E-Field polarization, and only in certain scan locations is BSE relatively insensitive to polarization variation; 2) given CP elements, radome-induced BSE is dependent on both aperture scan angle and reference E-Field polarization for all scan conditions under which BSE is non-zero; and 3) for sensitive/dependent BSE cases, the BSE exhibits "asymmetric" characteristics for polarization states where one might intuitively expect "symmetric" error.

Definitions of terms used in this effort are given in Section 2.1. Terms, such as "monopulse plane" and "polarization symmetry" are not common and will be defined in this effort. Other terms such as "BSE" and "ogive" have established definitions commonly used in a limited number of engineering fields.

Some basic electromagnetic-related theory is reviewed in Sections 2.2 and 2.3, including a simplified explanation for how a radome causes BSE. In Sections 2.4 and 2.5, the dependence of BSE on incident wave polarization is analyzed. This dependence is then extended by introducing a definition for polarization "symmetry".

The model and validation approach is described briefly in Chapter 3, along with minor changes to the original model. A more complete description of the original model, along with assumptions and underlying theory, is given in [1], and not repeated here.

Model results are given in Chapter 4, including initial validation data, as well as results for the polarization sensitivity and "asymmetric" variation cases. Both polarization dependence and "asymmetric" variation predicted in Section 2.5 are verified by the model.

2. Theory

2.1 Basic Definitions

2.1.1 Boresight Error (BSE)

Shown in Figure 1 is a target located in the direction of the unit normal $\hat{n}_{actual}$ and a radar-indicated direction given by the unit vector $\hat{n}_{indicated}$. The BSE is:

$$\theta_{BSE} = \cos^{-1}(\hat{n}_{actual} \cdot \hat{n}_{indicated}) \tag{1}$$

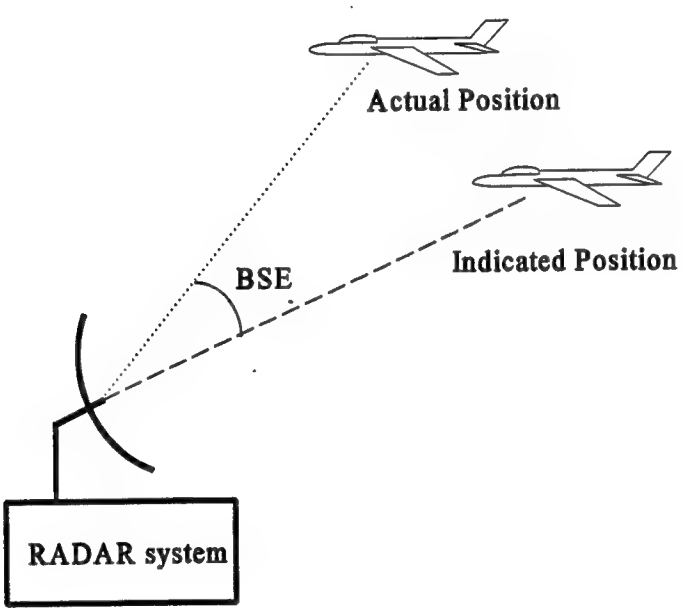

Figure 1 Graphical Depiction of BSE

Typical maximum BSE values for a production system may be on the order of 2.0 mRad, or 0.115°. For a target located at a range of 20 miles, this translates to a potential

position error of over 200 feet. This position error or miss distance could place the target aircraft outside the lethal range of a radar guided munition.

2.1.2 BSE Regions

BSE regions are aperture scan regions which are characterized by general BSE tendencies and radome distortion effects. Different analysis techniques apply in the different regions, so reference definitions will be required. The entire space over which the aperture scans may be divided into three regions, as shown in Figure 2. The regions described here are not limited to the ogive, but may be extended to other smooth, well-behaved shapes, such as cones and ellipsoids.

The distinction between the three regions is based on the behavior of the "aperture view" at a given scan location. Aperture view is defined as the aperture's projection on the radome, through which all rays emanating normal to the aperture plane must pass. (A radome axis of symmetry may be defined as an axis about which the radome can be defined as a body of revolution. Other shapes, which are not bodies of revolution, may also have an axis of symmetry, but these shapes are not examined in this effort. Some radome shapes have no axis of symmetry, while others have only one. A hemispheric radome represents a special case with an infinite number, since every possible surface normal defines an axis of symmetry. However, if the aperture gimbal point is not at the center of the sphere defining the hemispheric radome, the scan direction will generally not align with an axis of symmetry.)

The case when a scan angle is directed along a radome axis of symmetry will be called Region I. In this region, there is no radome-induced BSE because the "aperture

view" is symmetric about a radome axis of symmetry. For an ogive radome, Region I is limited to a single scan direction aligned with the radome nose, and the point at which the radome's axis of symmetry intercepts the radome surface (point A) is centered in the aperture view. The ogive shape is defined further in Section 2.1.5, but

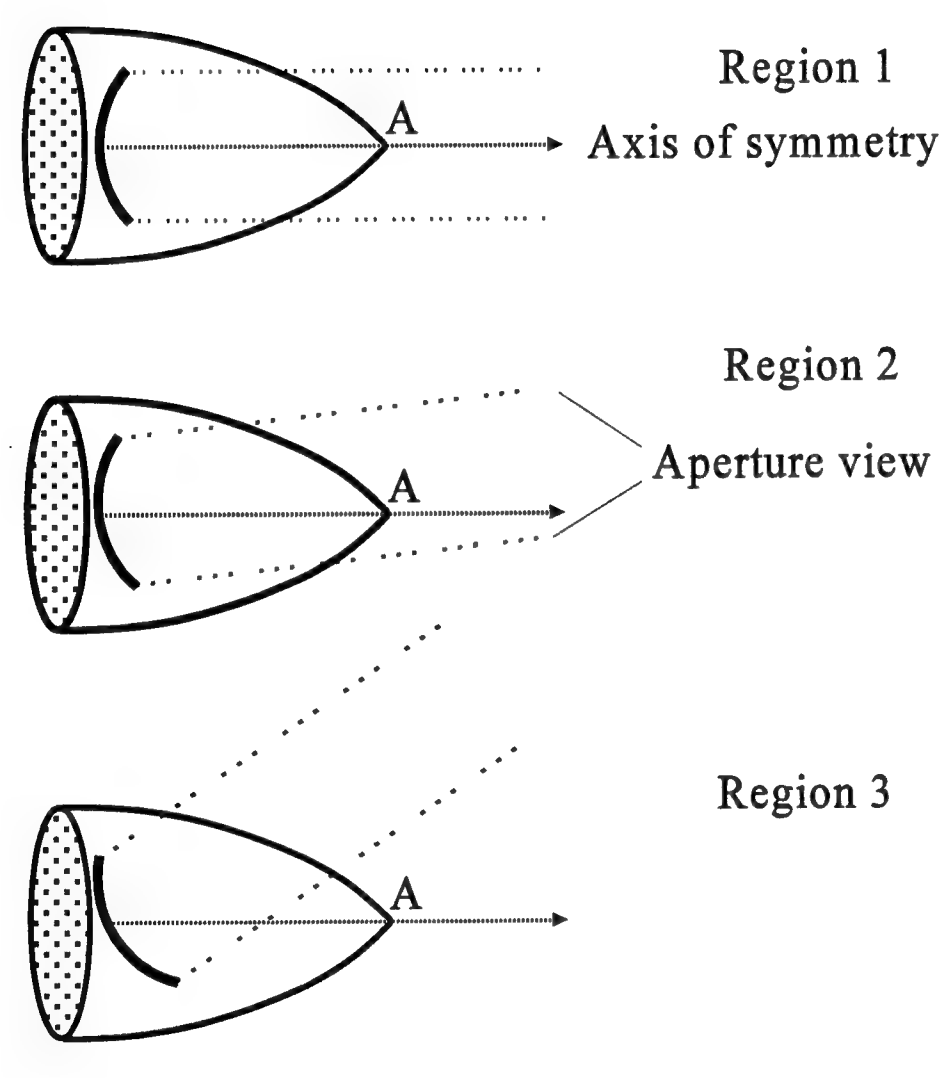

Figure 2 BSE Regions for an Ogive Radome

Figure 2 shows an ogive with the "Region I" direction clearly visible. For a hemispheric radome with the aperture gimballed at the center of the sphere, the entire possible scan range, through which the aperture does not view the edge of the radome, is Region I. This is a special case described in Section 4.4.2, in which there is no radome-induce BSE.

With the aperture scanned in Region I, all surface normals in the aperture view can be divided into four equal surface quadrants. For a coordinate system chosen such that the $+\hat{z}$ direction is aligned with the axis of symmetry and the quadrant divisions are aligned with the $\hat{x}$ and $\hat{y}$ axis, for every surface unit normal vector:

$$\hat{n}_1 = a\hat{x} + b\hat{y} + c\hat{z} \tag{2}$$

where a,b,c are direction cosines, there exist three corresponding points in the aperture view such that the respective unit normal vectors are given by:

$$\begin{aligned} \hat{n}_2 &= -a\hat{x} + b\hat{y} + c\hat{z} \\ \hat{n}_3 &= a\hat{x} - b\hat{y} + c\hat{z} \\ \hat{n}_4 &= -a\hat{x} - b\hat{y} + c\hat{z} \end{aligned} \tag{3}$$

All points in the Region I aperture view will have three corresponding points, one in each of the other three quadrants, so that given the surface normal described by (2) at some point, the surface normals at the corresponding points will satisfy (3). The set {(3) given (2)} is the set of all points on the radome surface for which all three of the corresponding points exist. In Region I, all points belong this set.

Region II is the angular region where the aperture scan direction is not aligned with an axis of symmetry, but the point at which the axis intercepts the radome is still contained within the aperture view. Point A is within the Region II aperture view, but not centered in it, as shown in Figure 2. This region presents a worst-case BSE condition, because the radome-induced distortion of amplitude, phase, and depolarization is the most uneven across the aperture. Not all points in the aperture view will belong to the set {(3) given (2)}, i.e. there will be at least one point with a surface normal given by (2), for which at least one condition of (3) cannot be satisfied by any of the points within the aperture view. However, if the radome surface is a body of revolution, and the aperture view is fixed, a coordinate system can be chosen such that all points not belonging to the set of {(3) given (2)} will instead have a single corresponding point, at which the surface normal satisfies one of the conditions in (4). These points belong to the set {(4) given (2)}.

$$\hat{n}_2 = -a\hat{x} + b\hat{y} + c\hat{z}$$
$$\textit{or} \qquad (4)$$
$$\hat{n}_2 = a\hat{x} - b\hat{y} + c\hat{z}$$

All points on a radome, whose shape is defined by a figure of revolution, will have all three corresponding points required for the set {(3) given (2)}, however, all four of the points may not be in the aperture view simultaneously. The aperture view contains only a subset of the total set of radome points, but the section of the radome surface, onto which the aperture view is projected, will have a curvature, symmetric about some line. This symmetry of curvature will ensure that, for all points for which the aperture view

does not contain all three corresponding points, at least one corresponding point will be included for some coordinate system. The locations of the three corresponding points are a function of the coordinate system orientation, with the x,y locations of each point reflected about the x and y axes for the corresponding points. It is possible to find a coordinate system to satisfy the requirements of {(4) given (2)}, since selecting an axis immediately adjacent to any point will place its corresponding point also immediately adjacent to the same axis, but just to the other side.

Region III is where the aperture view does not contain any radome axis of symmetry; point A is not within the aperture view. The distortion is less uneven because the aperture view is entirely across "one side" of the radome. The portion of the radome contained in the aperture view is relatively smooth and contains no sharp corners or points. For electrically large radomes, the radome surface at ray-radome intersection points more closely approximates planar surfaces. Given an ogive radome with the aperture scanned to Region III and an appropriately chosen coordinate system, all surface normals in the aperture view belong to the set {(4) given (2)}.

The unit normal relationships in Region I provide a symmetry which neutralizes the effects of radome-induced depolarization on BSE. In Regions II and III, the unit normal relationships provide only partial symmetry, allowing depolarization to directly affect BSE.

2.1.3 Monopulse Radar

One form of monopulse radar, phase monopulse, locates targets by using the phase information contained in a single radar pulse. If the aperture is wide with respect to the

radar wavelength and the target direction is slightly off to one side of aperture center, the electrical path length of a signal incident on one side of the aperture differs from the path length of the same signal incident on the other side. Although the magnitude of the incident signals are approximately equal across the aperture, the phase is not. This difference in phase is used to locate a target or source in a given angular direction relative to the aperture's mechanical boresight. Under ideal conditions, the phase difference is zero for targets on boresight.

A diagram of a monopulse receiver is shown in Figure 3, and the governing equations are:

$$V_{SUM}(\theta,\phi,\hat{p}_i) = \sum_{all\ elements} A_n e^{j\phi_n} f(\theta,\phi,\hat{p}_n)\vec{E}_n(\theta,\phi,\hat{p}_i)\cdot\hat{p}_n \tag{5}$$

$$V_{DEL}(\theta,\phi,\hat{p}_i) = \sum_{side1} A_n e^{j\phi_n} f(\theta,\phi,\hat{p}_n)\vec{E}_n(\theta,\phi,\hat{p}_i)\cdot\hat{p}_n - \sum_{side2} A_n e^{j\phi_n} f(\theta,\phi,\hat{p}_n)\vec{E}_n(\theta,\phi,\hat{p}_i)\cdot\hat{p}_n$$

where:

A_n, ϕ_n are the amplitude and phase weights of the n^{th} aperture element,

f is the element field pattern,

θ, ϕ are the polar and azimuth angles of scan,

$\hat{\mathbf{p}}_i$ is the polarization unit vector of the reference/incident E-Field,

$\hat{\mathbf{p}}_n$ is the polarization unit vector of the n^{th} aperture element,

$\mathbf{E}_n$ is the E-Field incident on the n^{th} element.

In addition, V_{DEL} may also have a phase shift, applying equally to all terms.

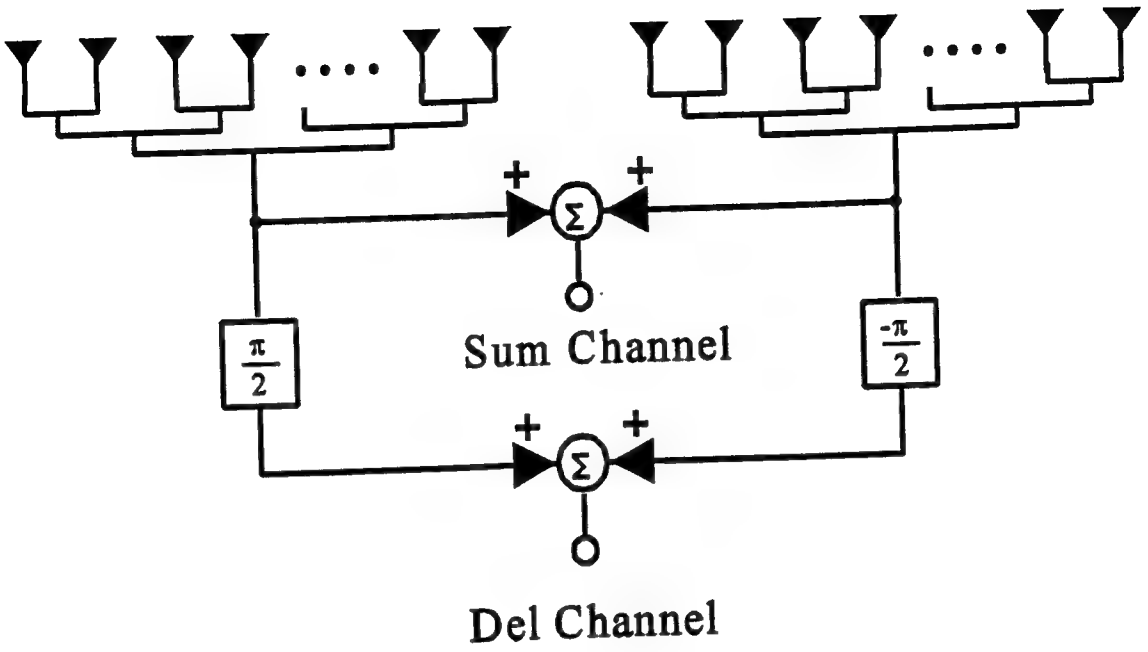

Figure 3 Monopulse Processing

When a target is on boresight and the system is ideal, each side of the aperture produces the same voltage and hence V_{DEL} is zero. In production monopulse systems, one defines an on-boresight condition by requiring the normalized difference voltage be zero.

$$MP_{err} = Re\left\{\frac{V_{DEL}}{V_{SUM}}\right\} = 0 \tag{6}$$

Due to noise and other production factors, the monopulse error signal is generated from the real part of the V_{DEL}/V_{SUM} ratio, as shown in (6), and the imaginary part is ignored [2:158].

A typical array sum pattern as a function of azimuth scan angle, while keeping all other parameters constant is shown in Figure 4. The aperture has been weighted to yield the side-lobe level shown.

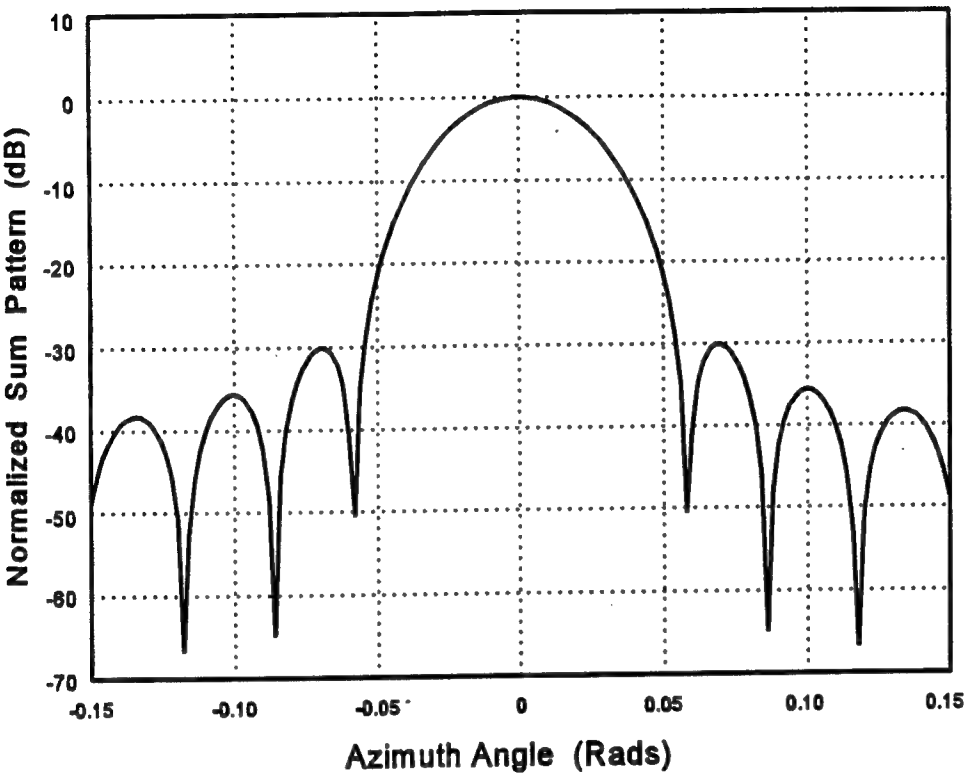

Figure 4 Typical Monopulse Sum Pattern

The normal angular range of operation for target acquisition is within the -3 dB beamwidth of the array sum pattern. The target must be within the main beam for monopulse processing, since within this angular region, the slope of the difference pattern, shown in Figure 5, is approximately linear. The difference pattern is normalized by:

$$V_{DIFF}(\theta) = \frac{|V_{DEL}(\theta)|}{|V_{SUM}(\theta = 0)|} \tag{7}$$

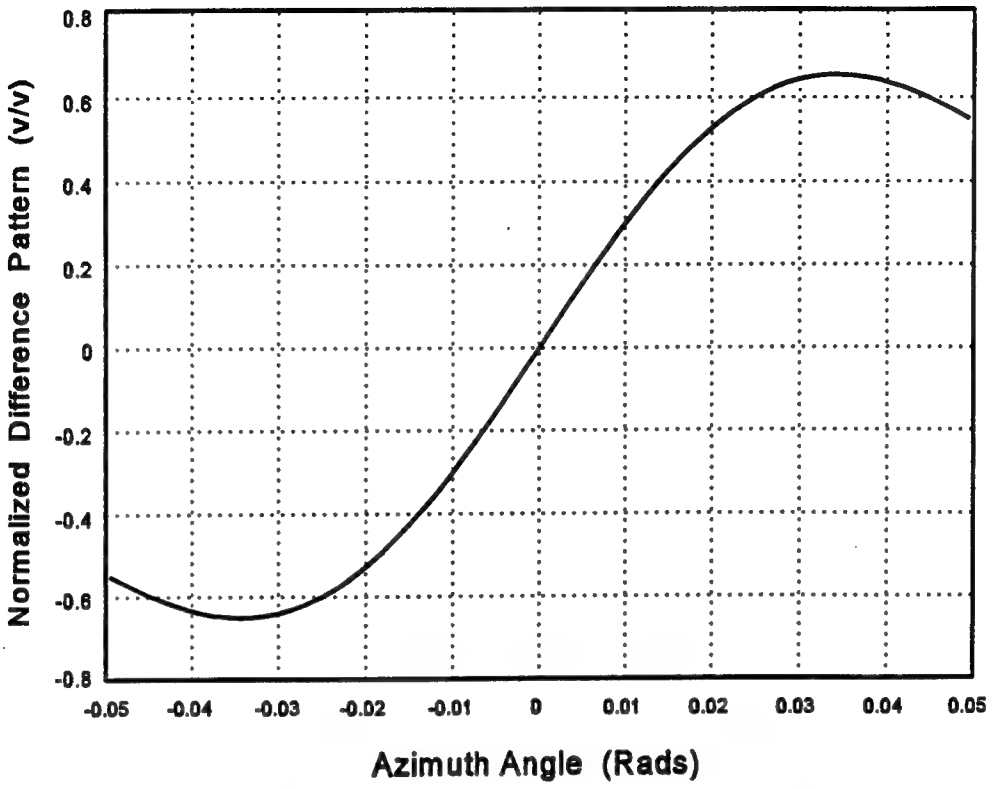

Figure 5 Typical Monopulse Difference Pattern

Since monopulse processing is performed within the angular region over which the S-curve is nearly linear, with the voltage of the difference signal is proportional to the target's angle off-boresight.

2.1.4 Monopulse Plane

The monopulse plane is the plane in which the projection of the target's direction is determined, and is orthogonal to the plane containing the aperture surface. Figure 6 shows an aperture divided into symmetric quadrants A through D. The aperture may be divided into halves two different ways. For quadrant A defined as the top left region,

{A+C} is the left half, {B+D} is the right half, or {A+B} is the top half, and {C+D} is the bottom half. With the proper circuitry, monopulse processing can be done two ways: Left/Right (L/R) or {A+C} versus {B+D}, and Top/Bottom (T/B) or {A+B} versus {C+D}. In this way, a single aperture can simultaneously perform both azimuth and elevation processing.

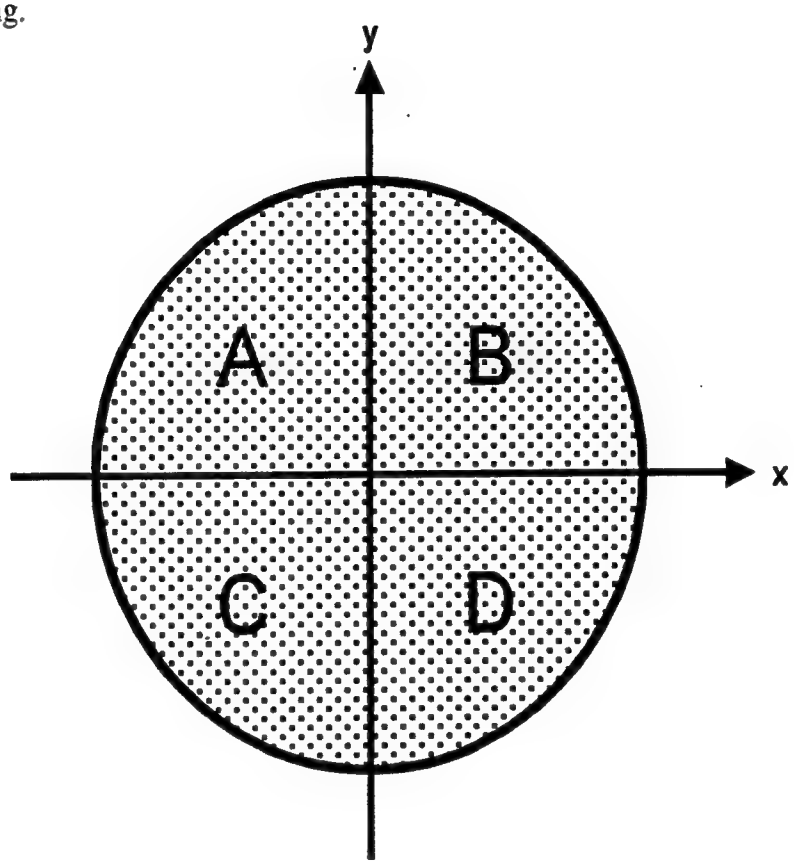

Figure 6 Four Quadrant Monopulse Regions

The L/R monopulse plane is orthogonal to the aperture, between the top and bottom halves, while the T/B monopulse plane separates the left and right sides. The two monopulse planes are orthogonal; the line defined by their intersection is the aperture's boresight.

2.1.5 Ogive Radome

The tangent ogive is shown in Figure 7. It is generated by revolving a circular arc such that one endpoint of the line remains fixed on the axis of revolution and the path traced by the other endpoint forms a circle in a plane orthogonal to the axis of revolution. The endpoint fixed on the axis is the tip, and the circular disk formed by the revolution of the other endpoint is the base. The arc's curvature is determined by a circle of radius R, whose center point lies in the plane containing the base. The arc has a length L projected on the axis of revolution and the width of the base is W.

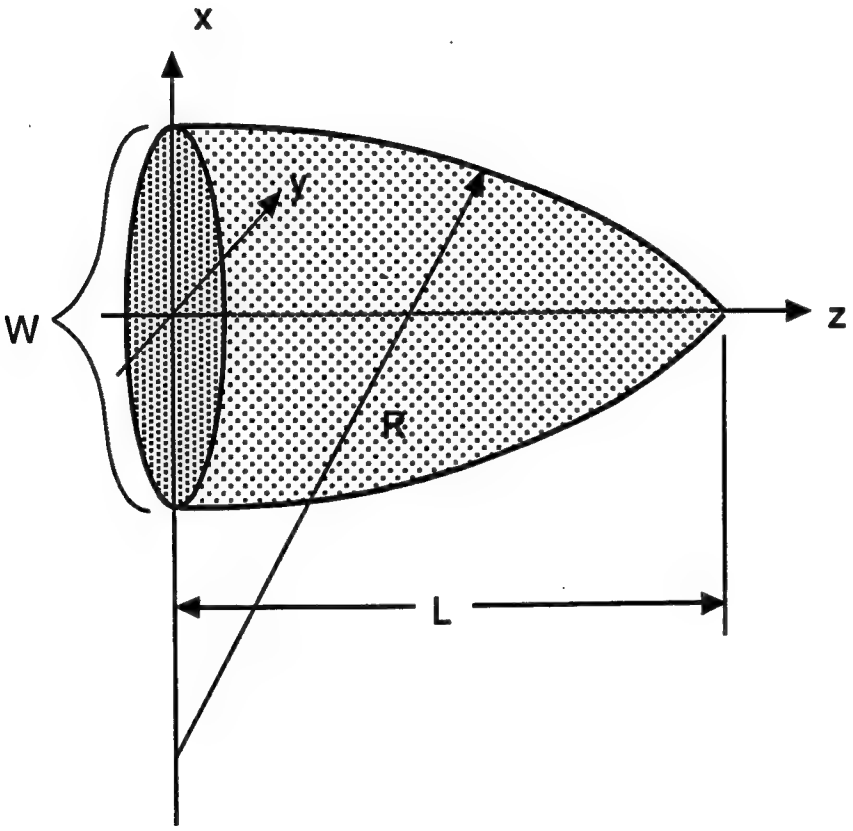

Figure 7 Tangent Ogive Radome

The ratio of length to width is the "fineness ratio", and for the radomes considered for this effort, the fineness ratio was approximately 3-to-1. A hemisphere is a special case of the general ogive shape, but with a fineness ratio of 1-to-2. This special case is evident from the governing equations:

$$L = \sqrt{R^2 - (R - \frac{W}{2})^2} \quad ; \quad R = \frac{L^2}{W} + \frac{W}{4} \tag{8}$$

Applying the fineness ratio of 1-to-2, W = 2L:

$$R = \frac{L^2}{2L} + \frac{2L}{4} = L \tag{9}$$

This provides the expected result, since a hemisphere's height, L in this case, is its radius, R, and its base width, W, is the sphere's diameter, 2R = 2L.

Ogive radomes are one of the most commonly used and modelled radome shapes [5]. It is an easily modeled shape, because it can be completely described by simple equations and specification of any two of: L, R, W, or fineness ratio.

2.1.6 Scan Plane

The scan plane is defined, for a given scan location, by the pair of vectors aligned with the aperture's mechanical boresight at both the scanned and unscanned position, and is perpendicular to the aperture plane. The arc connecting the aperture's unscanned and scanned mechanical boresight, therefore, also lies in the scan plane. For the coordinate

system in Figure 7, the unscanned boresight axis is the $\hat{z}$ axis, which is also the radome's axis of symmetry.

Considering Figure 7 a nearly top-down view of an ogive, the $\pm\hat{y}$ direction elevation, and the $\pm\hat{x}$ direction defines azimuth. If the aperture boresight is scanned off the $\hat{z}$ axis in the $+\hat{x}$ direction to an angle γ, and L/R monopulse processing is chosen, the scan plane and monopulse plane will be equal; both will be the y = 0 plane. Given the same scan location with T/B processing, the scan plane and monopulse plane will be orthogonal.

The relationship between the scan plane and the monopulse processing plane defines In-Plane (I-Plane) and Cross-Plane (X-Plane) BSE conditions. I-Plane BSE is the angular error contained in the scan plane while X-Plane BSE is angular error in the plane orthogonal to the scan plane. For example, if the aperture is scanned in azimuth, and L/R monopulse is performed, the resulting BSE is azimuth or I-Plane BSE. Given the same azimuth-only scan and T/B monopulse processing, the resulting BSE is elevation or X-Plane BSE.

2.1.7 Polarization and Depolarization

E-Field polarization is defined in the plane orthogonal to the field's direction of propagation. This plane is the polarization plane and is defined by any set of orthogonal unit vectors, $\hat{a}$ and $\hat{b}$, which satisfy:

$$\hat{a} \times \hat{b} = \hat{k} \tag{10}$$

where $\hat{k}$ is the unit vector in the direction of propagation.

Figure 8 represents a trace of the tip of the real part of an E-Field vector in the polarization plane, through an entire period [7:601]. The general trace pattern forms an ellipse, and can be described in terms of orthogonaly oriented components E_a and E_b. Each component of the E-Field may have its own initial phase, although the phase progression with either time or spatial propagation is identical for each component. In general, for a fixed position in space:

$$\begin{aligned} \vec{E}_{total} &= E_a e^{j\phi_a}\hat{a} + E_b e^{j\phi_b}\hat{b} \\ &= \left[E_a\hat{a} + E_b e^{j(\phi_b-\phi_a)}\hat{b}\right]e^{j\phi_a} \end{aligned} \tag{11}$$

where ϕ_a and ϕ_b are the phases of the individual components. Given two initial components of arbitrary phase and amplitude, a second set of two orthogonaly oriented components may be determined such that one, E_a, is aligned with the major axis of the ellipse and the other, E_b, aligned with the minor axis. The phase difference between these new components will be $\pm j$.

The expression given in (11) allows identification of several special cases: If the ϕ_a and ϕ_b of the initial set of E-Field components are equal or different by an integer multiple of π, the equivalent phase shift is zero, and the trace forms a single line. The length of the line would determine the magnitude of E_a, while E_b would be zero. This is LP, the polarization state used most often in this effort. Another special case occurs if E_a equals E_b when the phase difference is $\pm j$. For these conditions, the trace would form a circle and the resulting polarization state is CP. RCP occurs when the trace follows a clockwise rotation on the polarization plane, as viewed in the direction of

propagation (E_a - jE_b). LCP is a counter-clockwise trace rotation when viewed with the same perspective (E_a + jE_b).

Axial Ratio (AR) is the ratio of the lengths of the major and minor axes, its magnitude ranges from 1 for CP to ∞ for LP. The tilt angle, τ, is defined as the angle between the major axis of the polarization ellipse and some chosen axis. A tilt angle is not uniquely defined for CP E-Fields, since a circle has an infinite number of possible major axes.

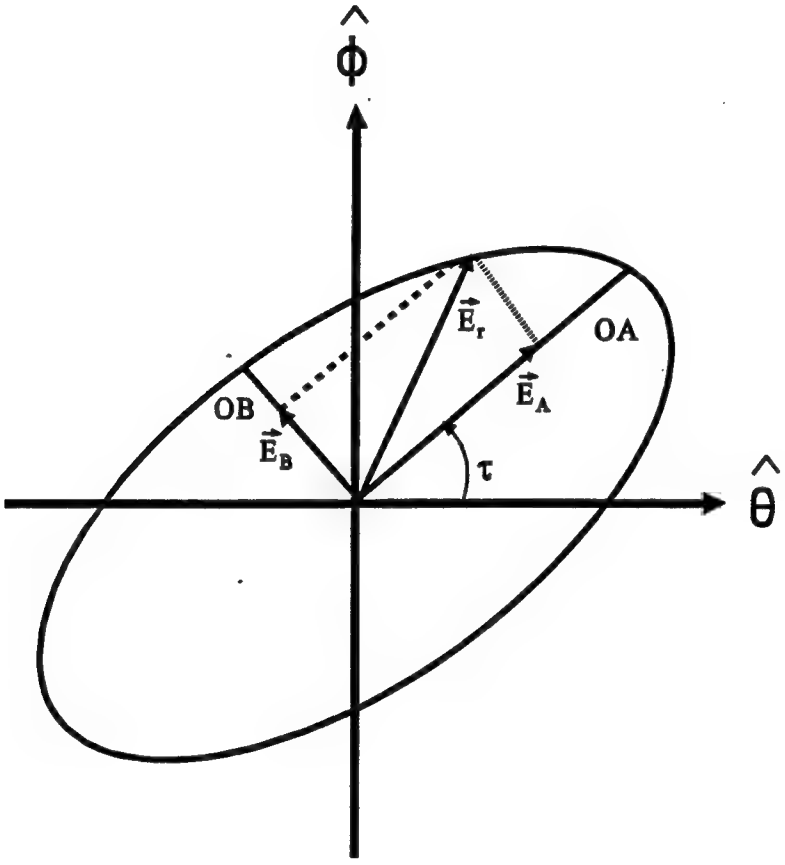

Figure 8 E-Field Polarization Ellipse

Depolarization is the net effect a radome has on changing an incident E-Field's polarization such that the transmitted E-Field possesses different polarization. Depolarization occurs when the AR, tilt angle, or both have been altered by the radome. Equivalent amplitude and phase shifts of both E-Field components (E_a and E_b) do not result in depolarization. However, if the E_a component is attenuated or phase shifted differently than the and E_b component, depolarization of the incident field occurs. Section 2.3 provides the explanation for this effect.

2.1.8 Polarization "Symmetry/Asymmetry"

An important use of polarization in this effort is verifying that a circularly symmetric radome surface introduces an "asymmetric" depolarization effect. The definition of asymmetric depolarization follows from the definition of symmetric polarization. Given an axis oriented along unit vector $\hat{a}$ and an orthogonal axis defined by $\hat{b}$, both in the polarization plane and satisfying (10), two E-Fields are defined as either "symmetrically" or "asymmetrically" polarized about $\hat{a}$ in the following manner: if two E-Fields have identical $\hat{a}$ components, and $\hat{b}$ components which are negatives of each other, as shown Figure 9, they are symmetrically polarized and may be expressed as in (12).

$$\vec{E}_1 = \alpha_1 \hat{a} + \beta_1 \hat{b} \quad ; \quad \vec{E}_2 = \alpha_2 \hat{a} + \beta_2 \hat{b}$$

$$\textit{if} \left\{ \begin{matrix} \alpha_1 = \alpha_2 = \alpha \\ \beta_1 = -\beta_2 = \beta \end{matrix} \right\} \textit{ then} \tag{12}$$

$$\vec{E}_1 = \alpha \hat{a} + \beta \hat{b} \quad ; \quad \vec{E}_2 = \alpha \hat{a} - \beta \hat{b}$$

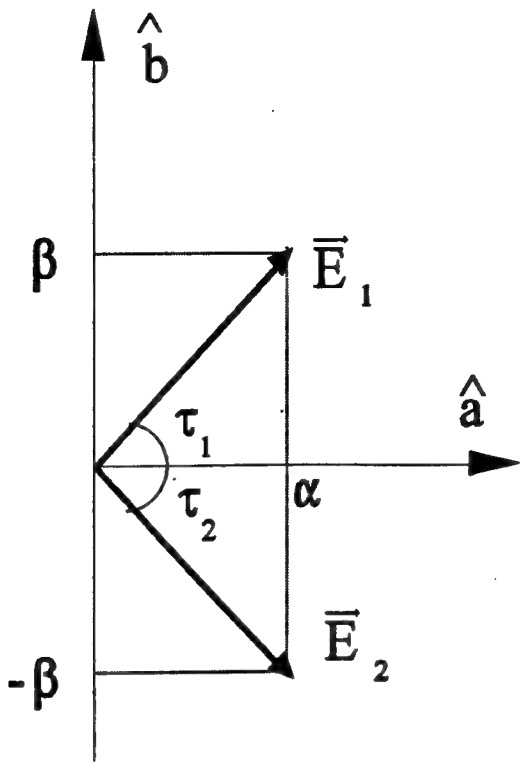

Figure 9 Symmetrically Polarized E-Fields

From Figure 9, tilt angles, τ_1 and τ_2, may be found per (13). Since defined relative to $\hat{a}$, the two tilt angles are the negative of each other, as shown in (14). The condition expressed in (14) represents a necessary, but not a sufficient, condition for "symmetry". To determine linearly polarized E-Field symmetry, (14) is first evaluated, and if not satisfied, the fields are declared "asymmetric". However, if (14) is true and both conditions expressed in (12) are satisfied, the fields are declared "symmetric". If (14) is satisfied, but (12) is not, the fields are "asymmetric" due to a scale factor.

$$\tau_1 = \cot^{-1}\frac{\alpha_1}{\beta_1} \quad ; \quad \tau_2 = \cot^{-1}\frac{\alpha_2}{\beta_2} \tag{13}$$

$$\tau_1 = -\tau_2 \quad \textit{because} \quad \frac{\alpha_1}{\beta_1} = -\frac{\alpha_2}{-\beta_2} \tag{14}$$

As defined, "symmetry" is dependent on the orientation of $\hat{a}$. Two E-Fields which are "symmetric" for a given direction of $\hat{a}$ may be "asymmetric" when the direction of $\hat{a}$ is changed.

Given the stated definition for symmetric polarization, "asymmetric depolarization" may be addressed. If two symmetrically polarized E-Fields are incident on a radome at a given point and corresponding transmitted E-Fields are not symmetrically polarized, as defined by (12), the depolarization is defined to be asymmetric. This is an important effect; the mechanics behind asymmetric depolarization are described in Section 2.4, with its implications further described in Section 2.5.

2.1.9 Parallel and Perpendicular Unit Vectors

A dielectric slab, such as a small section of a radome, will transmit and reflect an incident wave differently if its polarization is parallel versus perpendicular to the plane of incidence [7:613,616]. Therefore, it is important to be able to separate out the parallel and perpendicular components. To do this, the plane of incidence is first established. The plane of incidence is uniquely defined at each ray-radome intersection point, and is simultaneously orthogonal to both the reference E-Field polarization plane and the surface tangent plane at the intersection point. The plane of incidence is described by one in-plane unit vector, $\hat{u}_{||}$, and one orthogonal unit vector, $\hat{u}_{\perp}$. These two unit vectors, shown in Figure 10, are found from (15) using the definitions developed by Munk [8]. The

definitions were chosen so that the reflection coefficient for an E-Field incident on a perfect conductor is minus one.

$$\hat{u}_{\perp} = \frac{\hat{n} \times \hat{k}}{|\hat{n} \times \hat{k}|} \quad ; \quad \hat{u}_{||} = \hat{u}_{\perp} \times \hat{k} \tag{15}$$

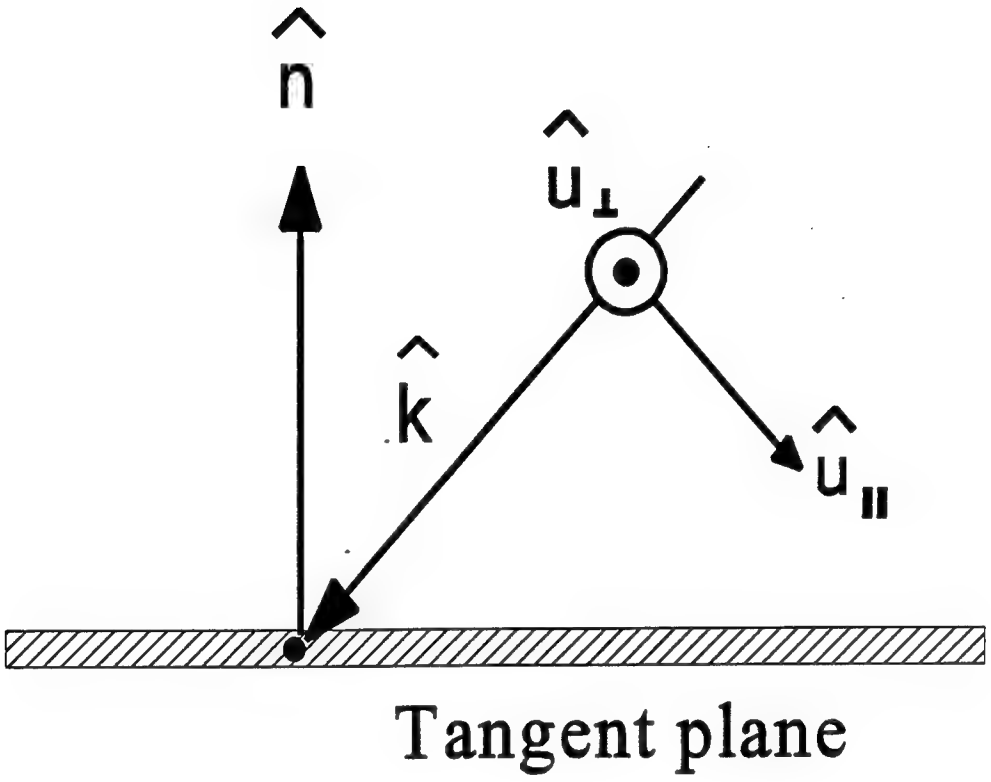

Figure 10 Unit Vectors in the Plane of Incidence

From Figure 10 and (15), the relationship given by (16) may be established. Comparison of (16) with (10) reveals that $\hat{a}$, $\hat{b}$, $\hat{u}_{||}$, and $\hat{u}_{\perp}$ are all co-planar.

$$\hat{u}_{||} \times \hat{u}_{\perp} = \hat{k} \tag{16}$$

Plane of incidence unit vectors, $\hat{u}_{||}$ and $\hat{u}_{\perp}$, are not constant over the surface of a radome, since their orientation is dependent on surface normal direction, i.e. $\hat{n}$ in (15) varies with position. However, all possible $\hat{u}_{||}$ and $\hat{u}_{\perp}$ pairs on the surface of the radome are co-planar since (16) must hold independent of position and $\hat{k}$ is constant.

2.2 Basic Theory

2.2.1 Geometric Optics (GO) Ray Tracing

GO ray tracing is an EM analysis technique useful for "electrically large" scatterers, i.e. object dimensions, radii of curvature, and distances are large compared to wavelength, λ. The radomes analyzed under this effort were at least 14λ in diameter at the base and up to 96λ in length.

Using GO, plane waves can be represented by a bundle of parallel E-Field rays spread across the region of interest. The energy density in a bundle of parallel rays is constant, with a spreading or converging bundle representing divergence or focusing of energy, respectively. All rays do not change direction until reflected, or refracted, and then continue on another straight path. This represents the propagating energy taking the shortest path between any two points, in accordance with Fermat's principle. Using the straight path rule, each ray can be traced from its point of origin, through interactions with dielectrics, reflectors, or other objects, while its phase, orientation and strength are tracked. Combining the results of a system's effects on all the rays in the original "plane wave" bundle indicates the systems overall effect on an incident plane wave, as shown in Figure 11.

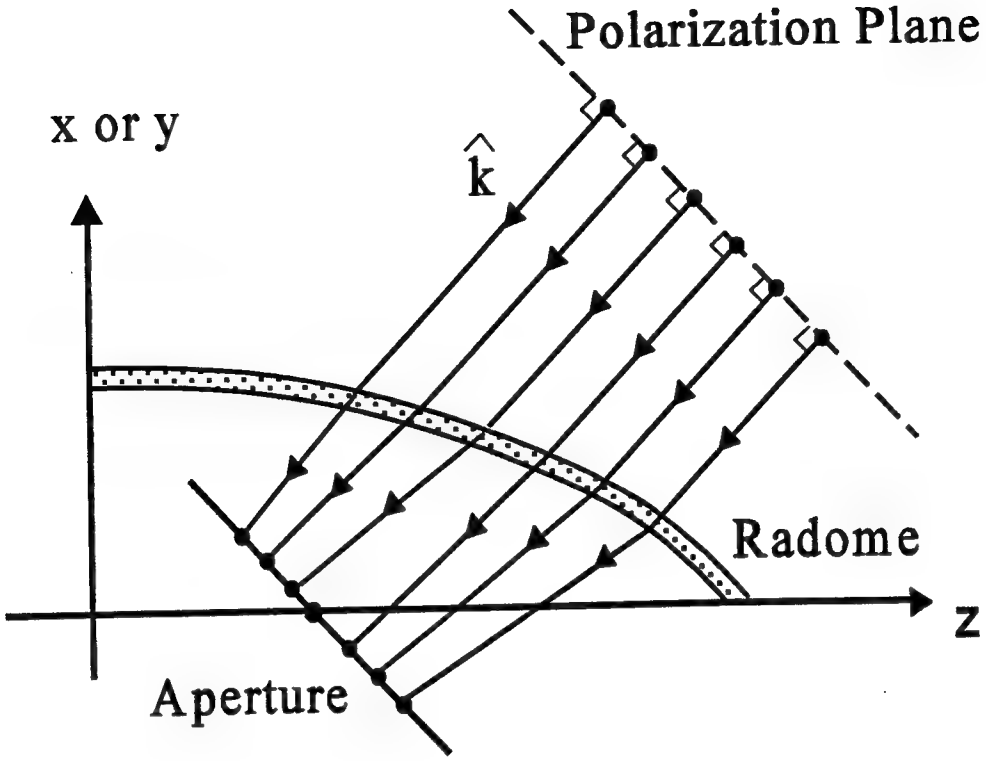

Figure 11 Go Ray Tracing

A perfect electric conductor (PEC) reflects the ray at an angle with the surface normal equal to the "angle of incidence", but on the opposite side of the normal and with a phase shift of π. The "angle of incidence" is the angle between the incident ray and the surface normal. A dielectric interface may reflect a portion of the ray and pass the remainder with a reduced strength, in an altered direction as given by Snell's Law, and with a different rate of phase progression with distance. The portion of a ray reflected from a dielectric interface becomes a new ray.

2.2.2 Transmission and Reflection Coefficients

The portions of a ray which are either transmitted through or reflected from a dielectric interface can be found through transmission and reflection coefficients, T and

Γ. In the simplest case, the strength of the transmitted ray is the incident ray's strength multiplied by T and the reflected ray's strength is the incident strength multiplied by Γ. However, T and Γ are functions of both the polarization of the incident ray and the angle the incidence as well as the dielectric properties. If the ray's polarization is such that the E-Field is contained entirely in the plane of incidence, the ray is Transverse Magnetic (TM). If the E-Field is orthogonal to the plane of incidence, the ray is Transverse Electric (TE). T and Γ are different for TE than for TM polarizations, and are given as:

$$T_{TE} = \frac{\cos(\theta_i) - \sqrt{\left(\frac{\varepsilon_2}{\varepsilon_1}\right) - \sin^2(\theta_i)}}{\cos(\theta_i) + \sqrt{\left(\frac{\varepsilon_2}{\varepsilon_1}\right) - \sin^2(\theta_i)}} \quad ; \qquad \Gamma_{TE} = 1 + T_{TE}$$

$$T_{TM} = \frac{-\left(\frac{\varepsilon_2}{\varepsilon_1}\right)\cos(\theta_i) + \sqrt{\left(\frac{\varepsilon_2}{\varepsilon_1}\right) - \sin^2(\theta_i)}}{\left(\frac{\varepsilon_2}{\varepsilon_1}\right)\cos(\theta_i) + \sqrt{\left(\frac{\varepsilon_2}{\varepsilon_1}\right) - \sin^2(\theta_i)}} \quad ; \qquad \Gamma_{TM} = 1 + T_{TM} \tag{17}$$

These coefficients are for a ray initially in a dielectric with relative permittivity ε_1 and entering a new dielectric with ε_2 at an angle of incidence θ_i. Plots of the Fresnel coefficients, T_{TE}, Γ_{TE}, T_{TM}, and Γ_{TM} are shown in Figures 12 and 13, respectively, for various ε_2's with ε_1 set to 1.0. A relative permittivity of exactly 1.0 occurs only in a vacuum, although air and some other materials may be close. For ε_1 and ε_2 both equal to 1.0, the transmission coefficients are both equal to 1.0, and the reflection coefficients are both equal to 0.0.

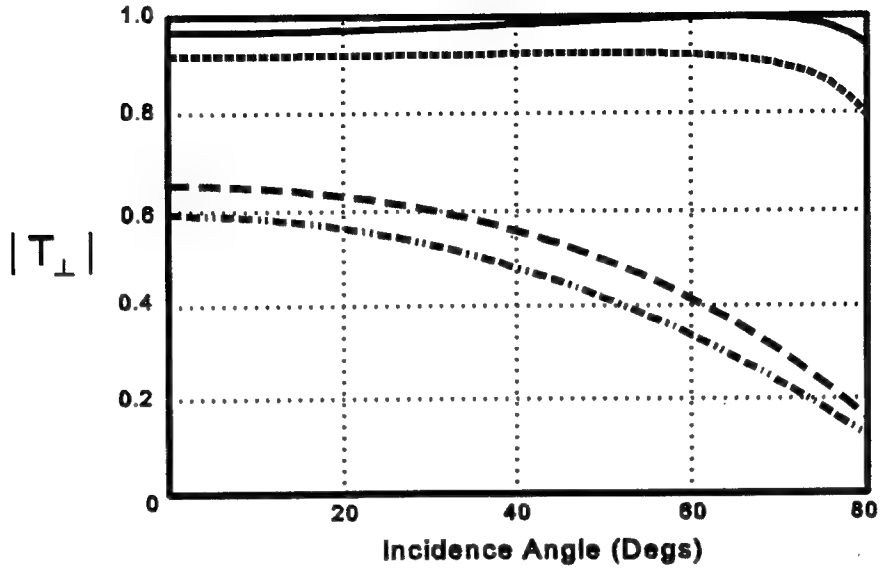

(a) Transmission

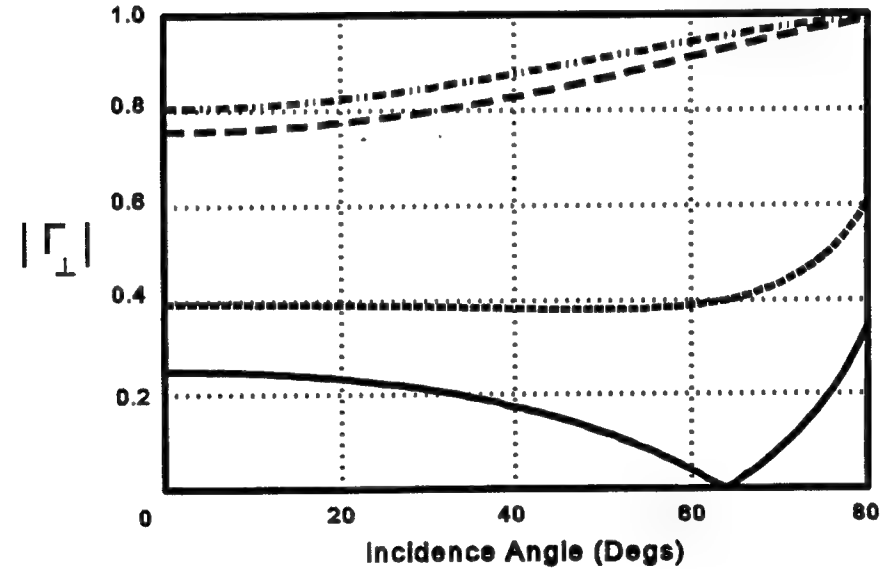

(b) Reflection

—— ϵ_r = 4.8 — — ϵ_r = 7.8

----- ϵ_r = 5.3 —·—·— ϵ_r = 9.3

Figure 12 TE Transmission and Reflection Coefficients

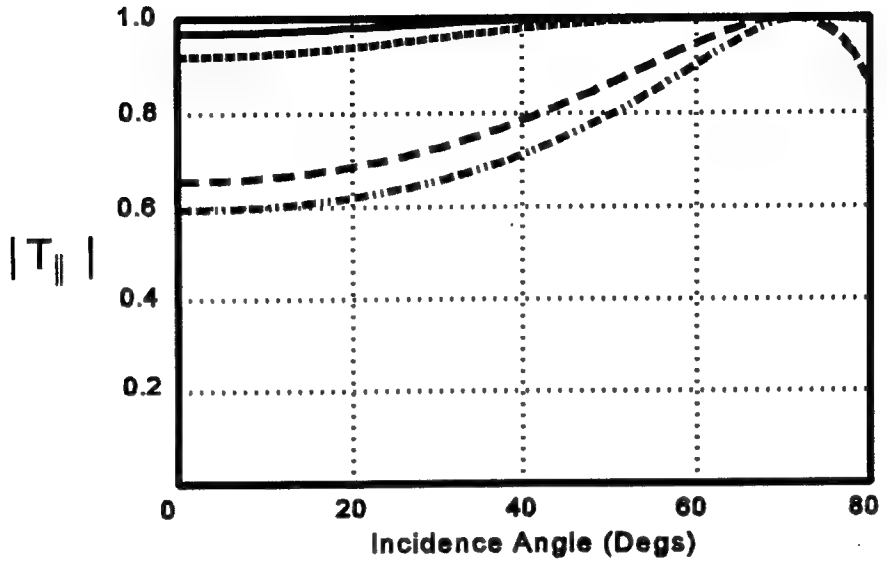

(a) Transmission

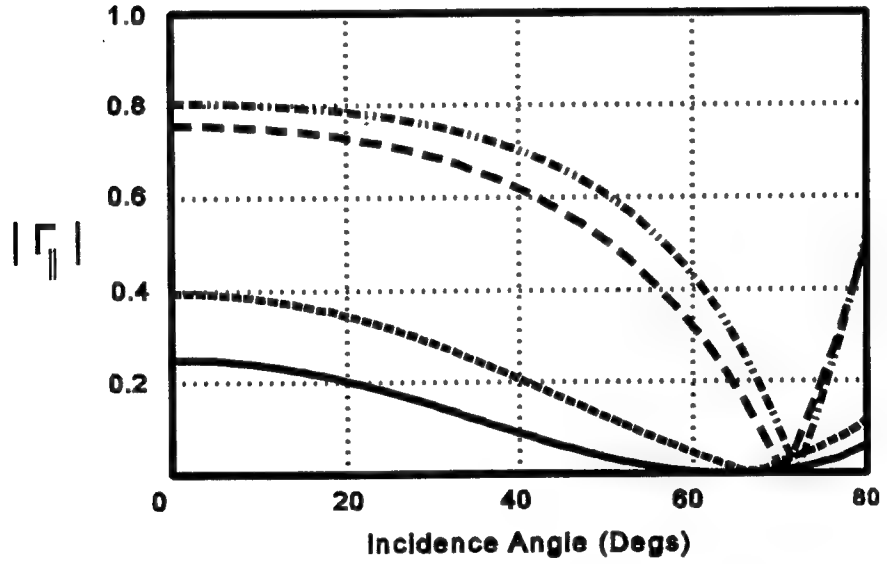

(b) Reflection

—— ε_r = 4.8 — — ε_r = 7.8

----- ε_r = 5.3 –·–·– ε_r = 9.3

Figure 13 TM Transmission and Reflection Coefficients

2.2.3 Simple Model of Radome-Induced BSE

A simple explanation of radome-induced BSE can be found by examining Figure 14 and applying (5) and (6) to a two element monopulse system. If no radome is present, then with some a common gain factor, the voltage of each element due to an incident E-Field may be expressed as:

$$e_1 = Ae^{-jk\left(R-\frac{d}{2}\right)} \quad ; \quad e_2 = Ae^{-jk\left(R+\frac{d}{2}\right)} \tag{18}$$

where A is the same amplitude for both elements, R is the distance from the object to the center of the aperture, and d is the path length difference from the elements to an off-center target.

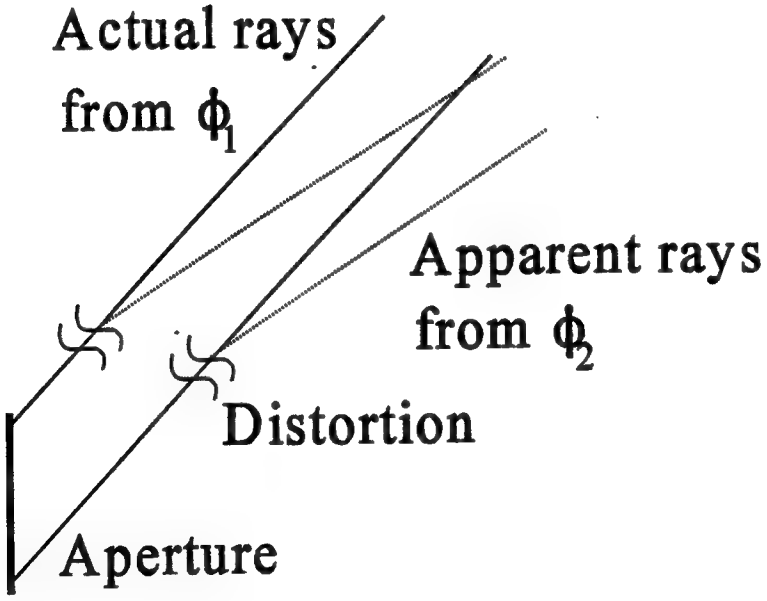

Figure 14 Simple Ray Distortion Model

The target is on boresight when both path lengths are equal, i.e. d = 0. This gives:

$$e_1 - e_2 = A\left(e^{-jkR} - e^{-jkR}\right) = 0 \tag{19}$$

However, if when a radome is added to the system, it may introduce uneven amplitude distortion, phase distortion, or depolarization. Consequently, the element voltages may be different from each other. For instance,

$$e_1 = A_1 e^{-jk\left(R-\frac{d}{2}\right)+\phi_1} \quad ; \quad e_2 = A_2 e^{-jk\left(R+\frac{d}{2}\right)+\phi_2}$$
$$A_1 \neq A_2 \quad \textit{and/or} \quad \phi_1 \neq \phi_2 \tag{20}$$

It is clear that (19) may not be satisfied for d = 0. Even for a target on boresight, (6) may not be satisfied, and the radar system will probably indicate the target to be at some non-zero angle relative to boresight.

2.3 Depolarization and Surface Refraction Effects

Depolarization, as explained in Section 2.1.6, is a primary cause of radome-induced BSE. A secondary cause is that of curved surface refraction, but it contributes negligible BSE variations for electrically large radar-radome systems [1].

2.3.1 Transverse Electric (TE) / Transverse Magnetic (TM) Effect

Generally, for a given angle of incidence, a dielectric slab will have different transmission coefficients for TE and TM fields, as depicted in Figures 12 and 13.

Arbitrarily oriented E-Fields are neither purely TE nor purely TM, but rather have a combination of TE and TM components. At each ray-radome intersection point, the incident E-Field is separated into TE and TM components, as shown in (21). Upon propagating through the radome, the TE and TM components, weighted by appropriate transmission coefficients, are recombined as shown in (22). From (22), the transmitted polarization state may be determined. The TE and TM radome transmission coefficients are complex quantities which generally are not equal to each other.

$$\begin{aligned} \vec{E}^i &= (\vec{E}^i \cdot \hat{u}_{||})\, \hat{u}_{||} + (\vec{E}^i \cdot \hat{u}_{\perp})\, \hat{u}_{\perp} \\ &= E^i_{TE}\, \hat{u}_{||} + E^i_{TM}\, \hat{u}_{\perp} \\ &= E^i_{||}\, \hat{u}_{||} + E^i_{\perp}\, \hat{u}_{\perp} \end{aligned} \tag{21}$$

$$\vec{E}^t = T_{||}\, E^i_{||}\, \hat{u}_{||} + T_{\perp}\, E^i_{\perp}\, \hat{u}_{\perp} \tag{22}$$

The complex TE/TM weighting effect has two important consequences, one due to the different coefficients at a single ray-radome intersection point, and another due to the variation in the weighting of the TE and TM components at different ray-radome intersection points. The single point consequence is "simple depolarization"; the transmitted E-Field possesses a different tilt angle than the incident E-Field, as shown in Figure 15. The second consequence results in an incident plane wave no longer being planar after passing through the radome. Since surface normal vectors vary with position, $\hat{u}_{||}$ and $\hat{u}_{\perp}$ also vary; the E-Field components of (21) are non-constant. This variation, along with the TE/TM relative weighting variation, result in the "simple depolarization" effect itself varying with position over the radome surface.

It is important to note that the transmission coefficients in (22) are not entirely the same as the coefficients for a plane wave incident on a simple dielectric half space, given in (17) and shown in Figures 12 and 13. The transmission coefficients used in the model and represented in (22) take into account the radome material loss tangent, thickness, and phase delay. The phase delay depends on the length of the path taken during transmission, and is different for each a single incidence angle with different ray-radome intersection points, and a single ray-radome intersection point with different incidence angles.

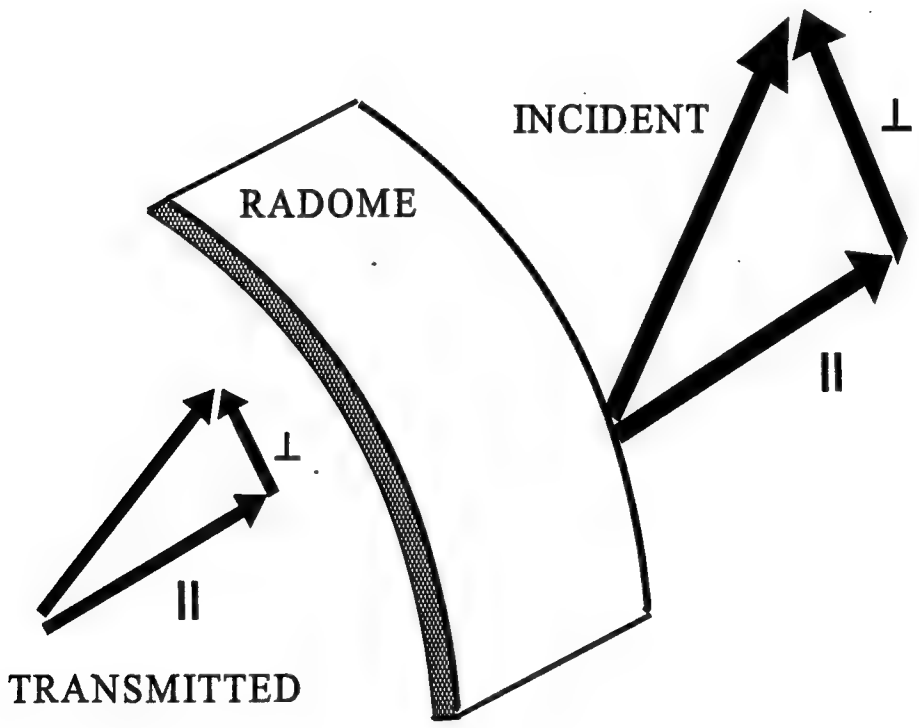

Figure 15 Graphical Representation of Radome Depolarization Effects

Some important features of a uniform plane wave (UPW) are 1) constant polarization, 2) constant amplitude, 3) constant phase, and 4) constant $\hat{k}$ over the entire plane. The TE/TM depolarization effect causes the transmitted E-Field to be a non-uniform plane wave, violating the first three conditions. Curved surface refraction effects, described in the next section, alter the propagation direction of the rays representing the incident plane wave in such a manner that they are no longer all parallel. This causes the transmitted E-Field to slightly violate the constant $\hat{k}$ condition. In general, a UPW incident on a radome will no longer be a UPW after transmission.

2.3.2 Curved Surface Refraction Effect

Upon passing through a planar dielectric slab, an incident ray will exit the slab and continue propagating in the incident direction (assuming the critical angle condition is not met). Given that incident and transmitted surface normals are parallel, the Snell's Law equations for refraction, (23) and (24), can be combined to form (25), where angles are measured from the same surface normal direction.

$$\sin\theta_d = \sqrt{\frac{1}{\epsilon_d}}\sin\theta_i \tag{23}$$

$$\sin\theta_t = \sqrt{\epsilon_d}\sin\theta_d \tag{24}$$

$$\sin\theta_t = \sqrt{\epsilon_d}\sqrt{\frac{1}{\epsilon_d}}\sin\theta_i = \sin\theta_i \quad ; \quad \theta_t = \theta_i \tag{25}$$

The symbol d denotes dielectric, i is incident, and t is transmitted.

One factor not apparent from (25) is the displacement of the ray inside the dielectric slab. Within the slab, the ray propagates at an angle different from the incident angle, and when it exits, it travels parallel to its original path, rather than resuming it. This can be seen in Figure 16, where the solid lines are the actual path and the dashed lines are the path the ray would have taken had the dielectric not been in place.

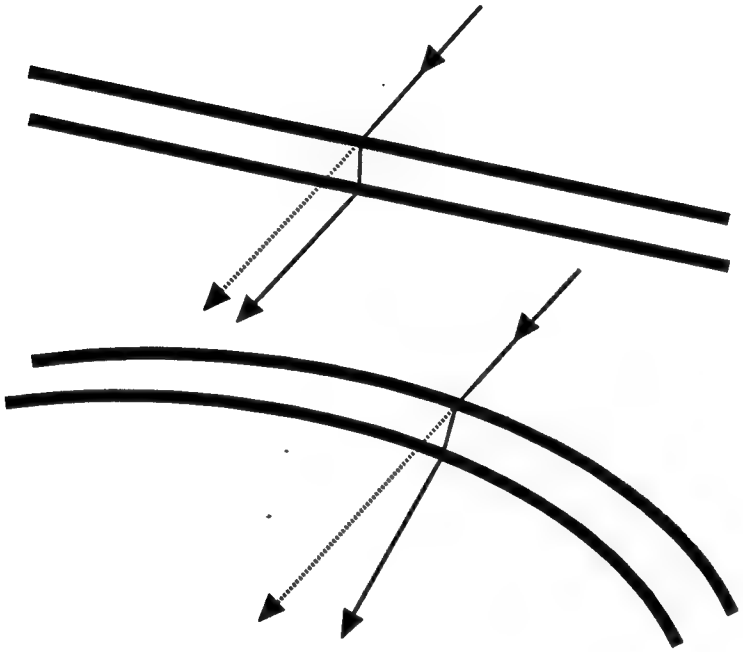

Figure 16 Flat versus Curved Surface Refraction Effects

The displacement is important, because when the surface is curved, (25) will not apply. When surface normal variations on a curved surface are factored into (23) and (24), the incident and transmitted propagation paths will be non-parallel. This second effect can also be seen, to an exaggerated extent, in Figure 16. Since different ray-

radome intersection points experience differing degrees of refraction, transmitted rays are non-parallel to the incident ray bundle and generally non-parallel to each other.

The dielectric materials used in production radomes have low relative permittivities and the radomes are thin compared to the radius of curvature. As a result, BSE due to refractive effects is very small when compared to BSE resulting from the depolarization effect. Although the computer model used in this research had the capability to include surface refraction effects for multi-layered radomes, BSE results for this effort have been obtained using no refraction. The difference in output BSE results were negligible when considering the additional execution time required [1:143].

2.4 Asymmetric Depolarization

To determine the nature of radome depolarization, the "simple depolarization" effect on a single ray with arbitrary strength, incidence angle, radome interception location, and polarization is examined. The goal is to develop a transmission function which can be applied to either a single pair of symmetrically polarized rays, intercepting the radome at a given point, or to a larger set of ray bundles representing two symmetrically polarized plane waves. A mathematical proof of asymmetric depolarization, as defined by (26) for LP only, and shown in Figure 17, is desired.

$$\begin{aligned} &\tau_2^i = -\tau_1^i \quad (\textit{symmetric incident}) \\ &\qquad \textit{but} \\ &\tau_2^t \neq -\tau_1^t \quad (\textit{asymmetric transmitted}) \end{aligned} \tag{26}$$

where τ represents the polarization tilt angles of the E-Fields shown.

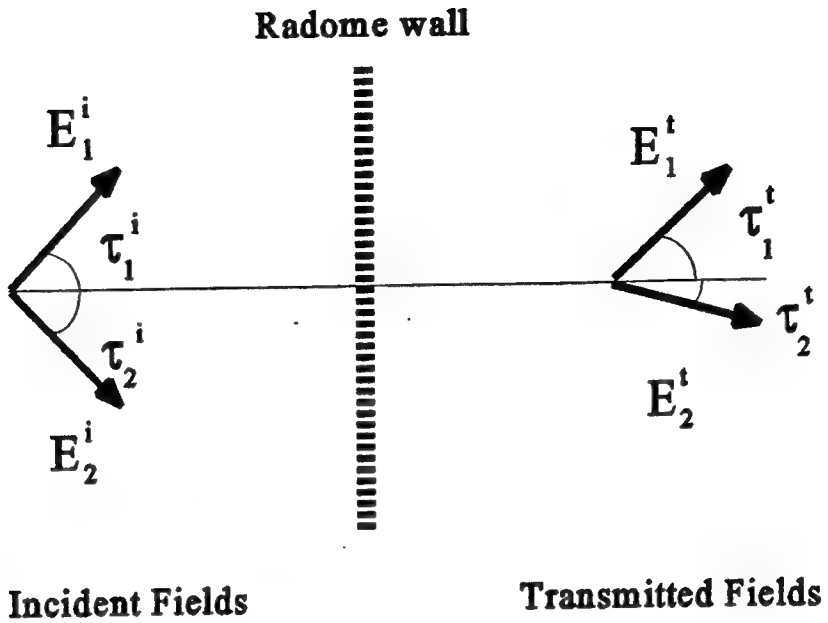

Figure 17 "Asymmetric" Depolarization Effect

2.4.1 Transmission Dyadic Development

To examine the effect of radome depolarization at a single ray-radome intersection point, a set of global unit vectors is used to describe the polarization orientation for both incident and transmitted E-Fields. In a previous development, it was noted that arbitrarily oriented unit vectors, $\hat{a}$ and $\hat{b}$, satisfying (10), and calculated unit vectors, $\hat{u}_{||}$ and $\hat{u}_{\perp}$, satisfying (15) and (16), all lie in the polarization plane if the incident ray. However, since $\hat{u}_{||}$ and $\hat{u}_{\perp}$ vary with position, they cannot be used to globally define the polarization of a plane wave. Therefore, arbitrary polarizations are described in terms of $\hat{a}$ and $\hat{b}$ on both the incident and transmitted side of the radome.

The "locally planar" approximation at ray-radome intersection points allows transmitted polarization states to be completely described in terms of $\hat{a}$ and $\hat{b}$ components.

Essentially, this approximation results in the polarization plane of the transmitted E-Field being parallel to the incident E-Field polarization plane, i.e. $\hat{k}_i = \hat{k}_t$.

The radome depolarization effect can be described by (27) where $\ddot{T}$ represents the transmission dyadic relating transmitted and incident E-fields. Decomposing the incident and transmitted fields into global $\hat{a}$ and $\hat{b}$ components, as shown in (28), results in the expression given by (29).

$$\vec{E}^t = \ddot{T} \cdot \vec{E}^i \tag{27}$$

$$\begin{aligned} \vec{E} &= (\vec{E}\cdot\hat{a})\,\hat{a} + (\vec{E}\cdot\hat{b})\,\hat{b} \\ &= E_a\,\hat{a} + E_b\,\hat{b} \end{aligned} \tag{28}$$

$$\begin{bmatrix} E_a^t \\ E_b^t \end{bmatrix} = \ddot{T} \begin{bmatrix} E_a^i \\ E_b^i \end{bmatrix} \tag{29}$$

The transmission dyadic will now be determined to characterize the depolarization effect. Considering a single ray-radome intersection point and using (28) in (21) gives:

$$\begin{aligned} \vec{E}^i = \; & (E_a^i \hat{a}\cdot\hat{u}_{||})\hat{u}_{||} + (E_b^i \hat{b}\cdot\hat{u}_{||})\hat{u}_{||} \\ & + (E_a^i \hat{a}\cdot\hat{u}_{\perp})\hat{u}_{\perp} + (E_b^i \hat{b}\cdot\hat{u}_{\perp})\hat{u}_{\perp} \end{aligned} \tag{30}$$

and applying (22):

$$\begin{aligned} \vec{E}^t = \; & E_a^i\,[T_{||}\,(\hat{a}\cdot\hat{u}_{||})\hat{u}_{||} + T_{\perp}\,(\hat{a}\cdot\hat{u}_{\perp})\hat{u}_{\perp}] \\ & + E_b^i\,[T_{||}\,(\hat{b}\cdot\hat{u}_{||})\hat{u}_{||} + T_{\perp}\,(\hat{b}\cdot\hat{u}_{\perp})\hat{u}_{\perp}] \end{aligned} \tag{31}$$

To find the polarization in terms of $\hat{a}$ and $\hat{b}$, (28) is applied a second time:

$$\begin{aligned}\vec{E}^t = \quad & \{E_a^i\,[T_{||}\,(\hat{a}\cdot\hat{u}_{||})(\hat{a}\cdot\hat{u}_{||}) + T_{\perp}\,(\hat{a}\cdot\hat{u}_{\perp})(\hat{a}\cdot\hat{u}_{\perp})] \\ & + E_b^i\,[T_{||}\,(\hat{b}\cdot\hat{u}_{||})(\hat{a}\cdot\hat{u}_{||}) + T_{\perp}\,(\hat{b}\cdot\hat{u}_{\perp})(\hat{a}\cdot\hat{u}_{\perp})]\}\,\hat{a} \\ + & \{E_a^i\,[T_{||}\,(\hat{a}\cdot\hat{u}_{||})(\hat{b}\cdot\hat{u}_{||}) + T_{\perp}\,(\hat{a}\cdot\hat{u}_{\perp})(\hat{b}\cdot\hat{u}_{\perp})] \\ & + E_b^i\,[T_{||}\,(\hat{b}\cdot\hat{u}_{||})(\hat{b}\cdot\hat{u}_{||}) + T_{\perp}\,(\hat{b}\cdot\hat{u}_{\perp})(\hat{b}\cdot\hat{u}_{\perp})]\}\,\hat{b}\end{aligned} \tag{32}$$

Expressing in the form of (29),

$$\begin{bmatrix} E_a^t \\ E_b^t \end{bmatrix} = \begin{bmatrix} T_{||}\,(\hat{a}\cdot\hat{u}_{||})^2 + T_{\perp}\,(\hat{a}\cdot\hat{u}_{\perp})^2 & T_{||}(\hat{a}\cdot\hat{u}_{||})(\hat{b}\cdot\hat{u}_{||}) + T_{\perp}(\hat{a}\cdot\hat{u}_{\perp})(\hat{b}\cdot\hat{u}_{\perp}) \\ T_{||}(\hat{a}\cdot\hat{u}_{||})(\hat{b}\cdot\hat{u}_{||}) + T_{\perp}(\hat{a}\cdot\hat{u}_{\perp})(\hat{b}\cdot\hat{u}_{\perp}) & T_{||}\,(\hat{b}\cdot\hat{u}_{||})^2 + T_{\perp}\,(\hat{b}\cdot\hat{u}_{\perp})^2 \end{bmatrix} \begin{bmatrix} E_a^i \\ E_b^i \end{bmatrix} \tag{33}$$

allows easy identification of the transmission dyadic:

$$\vec{\vec{T}} = \left[T_{||} \begin{bmatrix} (\hat{a}\cdot\hat{u}_{||})^2 & (\hat{a}\cdot\hat{u}_{||})(\hat{b}\cdot\hat{u}_{||}) \\ (\hat{a}\cdot\hat{u}_{||})(\hat{b}\cdot\hat{u}_{||}) & (\hat{b}\cdot\hat{u}_{||})^2 \end{bmatrix} + T_{\perp} \begin{bmatrix} (\hat{a}\cdot\hat{u}_{\perp})^2 & (\hat{a}\cdot\hat{u}_{\perp})(\hat{b}\cdot\hat{u}_{\perp}) \\ (\hat{a}\cdot\hat{u}_{\perp})(\hat{b}\cdot\hat{u}_{\perp}) & (\hat{b}\cdot\hat{u}_{\perp})^2 \end{bmatrix} \right] \tag{34}$$

The transmission dyadic is self-normalizing, i.e., it provides a maximum value of one for any incident polarization state. This is true because of two important relationships shown in (35) and (36). These equations hold true for all possible orientations of $\hat{a}$, $\hat{b}$, $\hat{u}_{||}$, and $\hat{u}_{\perp}$ given they are all coplanar unit vectors, $\hat{a}$ and $\hat{b}$ are orthogonal, and $\hat{u}_{||}$ and $\hat{u}_{\perp}$ are orthogonal. These constraints are enforced to satisfy (10) and (16).

$$\begin{aligned}(\hat{a}\cdot\hat{u}_{||})^2 + (\hat{a}\cdot\hat{u}_{\perp})^2 &= 1 \\ (\hat{b}\cdot\hat{u}_{||})^2 + (\hat{b}\cdot\hat{u}_{\perp})^2 &= 1\end{aligned} \tag{35}$$

$$(\hat{a}\cdot\hat{u}_{||})(\hat{b}\cdot\hat{u}_{||}) + (\hat{a}\cdot\hat{u}_{\perp})(\hat{b}\cdot\hat{u}_{\perp}) = 0 \tag{36}$$

Arbitrarily oriented unit vectors, satisfying the constraints mentioned above are shown in Figure 18, in order to verify (35) and (36). An arbitrary angle, γ, between $\hat{a}$ and $\hat{u}_{\perp}$, has been introduced for derivation purposes.

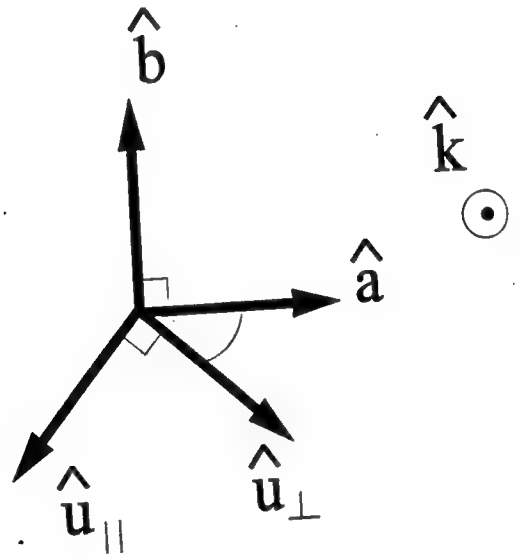

Figure 18 Unit Vector Relationships

Using a vector dot product:

$$\begin{aligned}
(\hat{a}\cdot\hat{u}_{||}) &= \cos(\gamma+90) &&= -\sin(\gamma)\\
(\hat{b}\cdot\hat{u}_{||}) &= \cos(90+\gamma+90) &&= -\cos(\gamma)\\
(\hat{a}\cdot\hat{u}_{\perp}) &= &&= \cos(\gamma)\\
(\hat{b}\cdot\hat{u}_{\perp}) &= \cos(90+\gamma) &&= -\sin(\gamma)
\end{aligned} \tag{37}$$

From the relationships in (37), (35) and (36) can be verified for all γ, i.e., for all permissible vector orientations, as shown in (38).

$$\begin{aligned}
(\hat{a}\cdot\hat{u}_{||})^2 + (\hat{a}\cdot\hat{u}_{\perp})^2 &= \sin^2(\gamma) + \cos^2(\gamma) &&= 1 \\
(\hat{b}\cdot\hat{u}_{||})^2 + (\hat{b}\cdot\hat{u}_{\perp})^2 &= \cos^2(\gamma) + \sin^2(\gamma) &&= 1 \\
(\hat{a}\cdot\hat{u}_{||})(\hat{b}\cdot\hat{u}_{||}) + (\hat{a}\cdot\hat{u}_{\perp})(\hat{b}\cdot\hat{u}_{\perp}) &= \sin(\gamma)\cos(\gamma) - \cos(\gamma)\sin(\gamma) &&= 0
\end{aligned} \tag{38}$$

2.4.2 Asymmetry of Transmission Dyadic

Depolarization symmetry is analyzed by considering transmission dyadic behavior for a pair of symmetrically polarized E-Fields incident at a given point on the radome. The symmetric pair of incident E-Fields considered for analysis are defined as given by (12), with final form:

$$\vec{E}_1^{\,i} = \alpha_0\,\hat{a} + \beta_0\,\hat{b} \quad ; \quad \vec{E}_2^{\,i} = \alpha_0\,\hat{a} - \beta_0\,\hat{b} \tag{39}$$

Using (28), the transmitted fields can be expressed as:

$$\vec{E}_1^{\,t} = E_{a1}^{t}\,\hat{a} + E_{b1}^{t}\,\hat{b} \quad ; \quad \vec{E}_2^{\,t} = E_{a2}^{t}\,\hat{a} + E_{b2}^{t}\,\hat{b} \tag{40}$$

The field components may be found by applying (33). This gives:

$$\begin{aligned}
E_{a1}^{t} = \alpha_1 &= T_{||}\,[\alpha_0(\hat{a}\cdot\hat{u}_{||})^2 + \beta_0(\hat{a}\cdot\hat{u}_{||})(\hat{b}\cdot\hat{u}_{||})] + T_{\perp}\,[\alpha_0(\hat{a}\cdot\hat{u}_{\perp})^2 + \beta_0(\hat{a}\cdot\hat{u}_{\perp})(\hat{b}\cdot\hat{u}_{\perp})] \\
E_{b1}^{t} = \beta_1 &= T_{||}\,[\alpha_0(\hat{a}\cdot\hat{u}_{||})(\hat{b}\cdot\hat{u}_{||}) + \beta_0(\hat{b}\cdot\hat{u}_{||})^2] + T_{\perp}\,[\alpha_0(\hat{a}\cdot\hat{u}_{\perp})(\hat{b}\cdot\hat{u}_{\perp}) + \beta_0(\hat{b}\cdot\hat{u}_{\perp})^2] \\
E_{a2}^{t} = \alpha_2 &= T_{||}\,[\alpha_0(\hat{a}\cdot\hat{u}_{||})^2 - \beta_0(\hat{a}\cdot\hat{u}_{||})(\hat{b}\cdot\hat{u}_{||})] + T_{\perp}\,[\alpha_0(\hat{a}\cdot\hat{u}_{\perp})^2 - \beta_0(\hat{a}\cdot\hat{u}_{\perp})(\hat{b}\cdot\hat{u}_{\perp})] \\
E_{b2}^{t} = \beta_2 &= T_{||}\,[\alpha_0(\hat{a}\cdot\hat{u}_{||})(\hat{b}\cdot\hat{u}_{||}) - \beta_0(\hat{b}\cdot\hat{u}_{||})^2] + T_{\perp}\,[\alpha_0(\hat{a}\cdot\hat{u}_{\perp})(\hat{b}\cdot\hat{u}_{\perp}) - \beta_0(\hat{b}\cdot\hat{u}_{\perp})^2]
\end{aligned} \tag{41}$$

For the transmitted fields to be symmetric, (12) must be satisfied. Applying the conditions of (12) to (41) yields the symmetric depolarization requirement of (42):

$$\{ \alpha_1 = \alpha_2 \text{ and } \beta_1 = \beta_2 \} \Rightarrow T_{||} (\hat{a}\cdot\hat{u}_{||})(\hat{b}\cdot\hat{u}_{||}) + T_{\perp} (\hat{a}\cdot\hat{u}_{\perp})(\hat{b}\cdot\hat{u}_{\perp}) = 0 \qquad (42)$$

Except for some special cases, (42) is generally not satisfied and the transmitted fields are asymmetric with respect to the given $\hat{a}$ and $\hat{b}$. One special case occurs when the parallel and perpendicular transmission coefficients are equal. In this case, (36) may be used to show that (42) is satisfied. Figures 12 and 13 indicate that this is an unlikely occurrence and can only be expected if the relative permittivity of the dielectric material is one, or the incidence angle is zero. A relative permittivity of one represents the special case of an air radome as discussed in Section 2.4.3. It is also possible that (42) will simply be satisfied at some point on the radome, due to the relative amounts of the dot products and transmission coefficients. But, since the transmission coefficients are complex and the dot products are real, exact cancellation will be unlikely.

Another special case in which (42) can be satisfied is when $\hat{a}$ or $\hat{b}$ are aligned with either $\pm\hat{u}_{||}$ or $\pm\hat{u}_{\perp}$. Given that $\hat{k}$ is specified and (10), (15), and (16) are satisfied, then from Figure 18:

$$\begin{aligned} &\textit{For} \quad \{ \hat{a} = \pm \hat{u}_{||} \Leftrightarrow \hat{b} = \pm \hat{u}_{\perp} \} \quad \textit{then} \quad \{ (\hat{a}\cdot\hat{u}_{\perp}) = 0 \textit{ and } (\hat{b}\cdot\hat{u}_{||}) = 0 \} \\ &\textit{For} \quad \{ \hat{a} = \pm \hat{u}_{\perp} \Leftrightarrow \hat{b} = \mp \hat{u}_{||} \} \quad \textit{then} \quad \{ (\hat{a}\cdot\hat{u}_{||}) = 0 \textit{ and } (\hat{b}\cdot\hat{u}_{\perp}) = 0 \} \end{aligned} \qquad (43)$$

Existence of a solution under these conditions leads to the following conclusion: given propagation direction $\hat{k}$ and any point on the radome surface, there exist four

possible sets of perpendicular unit vectors $\hat{a}$ and $\hat{b}$ in the polarization plane such that (43) is satisfied, i.e., either $\hat{a}$ or $\hat{b}$ lie in the plane of incidence. Incident E-Field ray pairs, symmetrically polarized about any of these constrained directions of $\hat{a}$, will produce symmetrically polarized transmitted E-Fields when incident at any of these points. To determine one of the four possible orientations of $\hat{a}$ and $\hat{b}$, it is possible to specify $\hat{k}$, $\hat{a}$, and $\hat{b}$, and determine the locus of points such that (43) is satisfied, i.e., find all points on the radome lying in a plane of incidence parallel to either $\hat{a}$ or $\hat{b}$. The locus of these points will form four arcs on the radome surface, emanating from the nose to the base, and perpendicular to each other at the nose.

When the plane of incidence is determined at a point on the radome, for a given $\hat{k}$, the plane "cuts" the radome and contains a 2-D cross-sectional "slice" of the radome shape, as shown in Figure 19. For any circularly symmetric radome shape, such as an ogive, this "slice" contains two arcs, each extending from the tip of the radome to the radome base. All points on the radome lying in the plane of incidence and contained on one of the two arcs, have identical $\hat{u}_{||}$ and $\hat{u}_{\perp}$. The $\hat{u}_{||}$ and $\hat{u}_{\perp}$ on one of the arcs are the negatives of the $\hat{u}_{||}$ and $\hat{u}_{\perp}$ on the other arc. This relationship is evident in Figure 19.

If (43) is satisfied at any one of the ray-radome intersection points in the given plane of incidence, it will be satisfied for all other points in the same plane of incidence, or all other points on the same arc. If a second plane is considered, orthogonal to the given plane of incidence, and positioned such that the intersection of the two planes is on the radome's axis of symmetry, it will be a complementary plane of incidence, with a similar 2-D projection of the radome, such that the $\hat{u}_{||}$'s and $\hat{u}_{\perp}$'s in the original plane

of incidence become the $\hat{u}_{\perp}$'s and $\hat{u}_{||}$'s in the complementary plane, respectively. If (43) is satisfied in the original plane of incidence, it will be satisfied in the complementary plane of incidence, i.e., if $\hat{a}$ lies in the original plane of incidence, $\hat{b}$ lies in the complementary plane of incidence and vice versa.

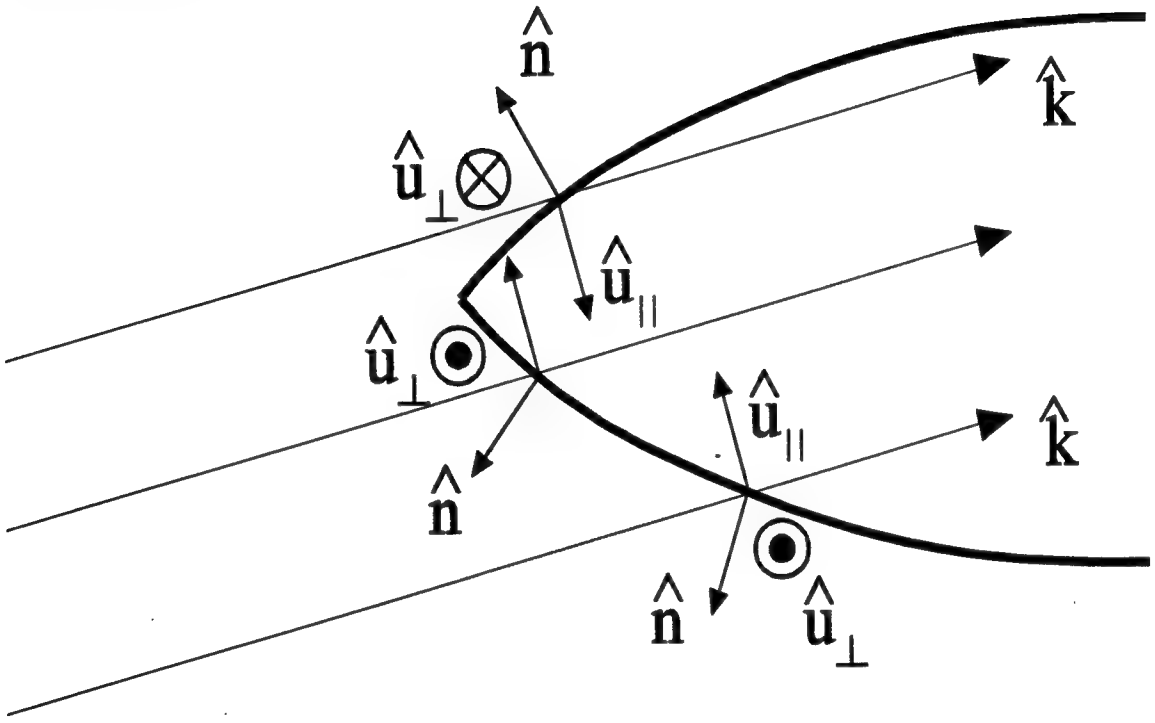

Figure 19 Ogive Projection on Plane of Incidence

For a given $\hat{k}$, $\hat{a}$, and $\hat{b}$, four curved line segments will exist, extending from the tip of the radome to its base, their projections aligned with the projections of $\pm\hat{a}$ and $\pm\hat{b}$ in the plane orthogonal to the radome's axis of symmetry, such that (42) is satisfied via (43). All rays incident on the radome at points contained in those line segments will be symmetrically depolarized. However, the incident plane wave is represented by a bundle

of parallel rays, spread across the entire aperture. Although it is possible for a limited number of the rays to intersect the radome on the four line segments, the majority will not intersect one of these line segments and will therefore experience asymmetric depolarization.

2.4.3 Special Case: Air Radome

For the special case of an air radome, i.e., a lossless dielectric radome with a relative permittivity and permeability of 1.0, the TE and TM transmission coefficients equal to 1.0 for all incidence angles. As a result, (42) is identically satisfied via (36), and the transmission dyadic in (34) becomes:

$$\ddot{T} = \begin{bmatrix} (\hat{a}\cdot\hat{u}_{||})^2 & (\hat{a}\cdot\hat{u}_{||})(\hat{b}\cdot\hat{u}_{||}) \\ (\hat{a}\cdot\hat{u}_{||})(\hat{b}\cdot\hat{u}_{||}) & (\hat{b}\cdot\hat{u}_{||})^2 \end{bmatrix} + \begin{bmatrix} (\hat{a}\cdot\hat{u}_{\perp})^2 & (\hat{a}\cdot\hat{u}_{\perp})(\hat{b}\cdot\hat{u}_{\perp}) \\ (\hat{a}\cdot\hat{u}_{\perp})(\hat{b}\cdot\hat{u}_{\perp}) & (\hat{b}\cdot\hat{u}_{\perp})^2 \end{bmatrix} \tag{44}$$

Applying (35) and (36):

$$\ddot{T} = \begin{bmatrix} 1 & 0 \\ 0 & 1 \end{bmatrix} \tag{45}$$

the transmitted field can be found by (29) to be:

$$\begin{bmatrix} E_a^t \\ E_b^t \end{bmatrix} = \begin{bmatrix} 1 & 0 \\ 0 & 1 \end{bmatrix} \begin{bmatrix} E_a^i \\ E_b^i \end{bmatrix} \quad ; \quad \vec{E}^t = \vec{E}^i \tag{46}$$

From (46) it is evident that the transmitted field is identical to the incident field and there is no radome-induced depolarization Since the air radome does not depolarize the incident field, there is no radome-induced distortion and no radome-induced BSE. This result is expected, since an air radome is equivalent to no radome at all.

2.5 Asymmetric BSE

If two plane waves, symmetrically polarized when incident on the radome, produce different BSE values at a given aperture scan position, the BSE is defined as "asymmetric". Asymmetric BSE is due to asymmetric depolarization, i.e., incident symmetric E-Fields lose polarization symmetry upon propagating through the radome. The resulting variations in transmitted E-Field polarization produce variations in BSE.

To examine the effect of polarization on BSE, a two element monopulse system is introduced. Combining (5) and (6) for a L/R monopulse system (and introducing the monopulse error signal) gives:

$$MP_{err}(\theta,\phi,\hat{p}_i) = Re\left\{\frac{\frac{\pi}{2}\left[\sum_{Left} A_n e^{j\Phi_n}\vec{E}_n(\theta,\phi,\hat{p}_i)\cdot\hat{p}_n - \sum_{Right} A_n e^{j\Phi_n}\vec{E}_n(\theta,\phi,\hat{p}_i)\cdot\hat{p}_n\right]}{\sum_{all\ elements} A_n e^{j\Phi_n}\vec{E}_n(\theta,\phi,\hat{p}_i)\cdot\hat{p}_n}\right\} \quad (47)$$

where θ and ϕ are polar angles which determine the scan location and $\hat{p}_i$ is the incident E-Field polarization. If the system has no BSE, MP_{err} = 0.0. The MP_{err} signal is introduced for a comparison of error values under various incident polarization conditions.

Assuming all elements have identical phase delays (mechanically scanned aperture) and polarizations, $\hat{p}_e$, and the aperture scan position is fixed, (47) can be simplified:

$$MP_{err}(\hat{p}_i) = Re\left\{ \frac{\left[\sum_{Left} A_n \vec{E}_n(\hat{p}_i) - \sum_{Right} A_n \vec{E}_n(\hat{p}_i)\right] \cdot \hat{p}_e}{\left[\sum_{Left} A_n \vec{E}_n(\hat{p}_i) + \sum_{Right} A_n \vec{E}_n(\hat{p}_i)\right] \cdot \hat{p}_e} \right\} \tag{48}$$

The numerator and denominator in (48) can each be replaced with a single vector:

$$\begin{aligned} \vec{E}_{Left} &= \sum_{Left} A_n \vec{E}_n(\hat{p}_i) \\ \vec{E}_{Right} &= \sum_{Right} A_n \vec{E}_n(\hat{p}_i) \end{aligned} \tag{49}$$

Separating the combined voltage terms into the global unit vector components yields:

$$\begin{aligned} \vec{E}_{Left} &= (\vec{E}_{Left} \cdot \hat{a})\hat{a} + (\vec{E}_{Left} \cdot \hat{b})\hat{b} \\ &= \alpha_L \hat{a} + \beta_L \hat{b} \\ \vec{E}_{Right} &= (\vec{E}_{Right} \cdot \hat{a})\hat{a} + (\vec{E}_{Right} \cdot \hat{b})\hat{b} \\ &= \alpha_R \hat{a} + \beta_R \hat{b} \end{aligned} \tag{50}$$

Using this result, (48) may be simplified as:

$$MP_{err}(\hat{p}_i) = Re\left\{ \frac{\left[(\alpha_L - \alpha_R)\hat{a} + (\beta_L - \beta_R)\hat{b}\right] \cdot \hat{p}_e}{\left[(\alpha_L + \alpha_R)\hat{a} + (\beta_L + \beta_R)\hat{b}\right] \cdot \hat{p}_e} \right\} \tag{51}$$

The dependence of BSE on both element polarization and a net transmitted E-Field equivalent polarization is obvious from (51). The net transmitted E-Field equivalent polarization can be found from the weighted sums of the polarization components of all rays incident on each portion of the aperture; this is addressed in Section 2.5.1.

BSE response to symmetrically polarized reference E-Fields can be examined using (51). For two symmetrically polarized incident E-Fields, E_1 and E_2, no assumption is made as to the symmetry of their net equivalent transmitted polarization. The transmitted E-Field equivalents can be represented as in (50):

$$\begin{aligned} \vec{E}_{Left1} &= \alpha_{L1}\,\hat{a} + \beta_{L1}\,\hat{b} \quad ; \quad \vec{E}_{Left2} = \alpha_{L2}\,\hat{a} + \beta_{L2}\,\hat{b} \\ \vec{E}_{Right1} &= \alpha_{R1}\,\hat{a} + \beta_{R1}\,\hat{b} \quad ; \quad \vec{E}_{Right2} = \alpha_{R2}\,\hat{a} + \beta_{R2}\,\hat{b} \end{aligned} \tag{52}$$

Each E-Field polarization case, E_1 and E_2, will produce an error value, $MPerr_1$ and $MPerr_2$. If the BSE values are the same for the symmetric polarizations,

$$\begin{aligned} MP_{err1}(\hat{p}_1) &= MP_{err2}(\hat{p}_2) \\ MP_{err1}(\hat{p}_1) - MP_{err2}(\hat{p}_2) &= 0 \end{aligned} \tag{53}$$

Using (52) in (51), and applying (53) gives the symmetric BSE requirement:

$$Re\left\{ \frac{\left[\left[(\alpha_{L1} - \alpha_{L2}) - (\alpha_{R1} - \alpha_{R2})\right]\hat{a} + \left[(\beta_{L1} - \beta_{L2}) - (\beta_{R1} - \beta_{R2})\right]\hat{b}\right]\cdot\hat{p}_e}{\left[\left[(\alpha_{L1} - \alpha_{L2}) + (\alpha_{R1} - \alpha_{R2})\right]\hat{a} + \left[(\beta_{L1} - \beta_{L2}) + (\beta_{R1} - \beta_{R2})\right]\hat{b}\right]\cdot\hat{p}_e} \right\} = 0 \tag{54}$$

In the case of symmetric BSE, there will be no variation with polarization at all; BSE is either asymmetric with polarization, or entirely insensitive. Two possible solutions for (54) are given by:

$$\begin{gathered} \alpha_{L1} = \alpha_{L2} = \alpha_{R1} = \alpha_{R2} \\ \textit{and} \\ \beta_{L1} = -\beta_{L2} = \beta_{R1} = -\beta_{R2} \end{gathered} \tag{55}$$

or

$$\begin{gathered} \alpha_{L1} = \alpha_{L2} \quad \textit{and} \quad \alpha_{R1} = \alpha_{R2} \quad \textit{and} \quad (\hat{p}_e \cdot \hat{b}) = 0 \\ \textit{or} \\ \beta_{L1} = \beta_{R1} \quad \textit{and} \quad \beta_{L2} = \beta_{R2} \quad \textit{and} \quad (\hat{p}_e \cdot \hat{a}) = 0 \end{gathered} \tag{56}$$

The condition shown in (55) is "net symmetric depolarization", i.e., the net equivalent fields as given in (49) satisfy the requirements for symmetric depolarization, even though individual rays may not. The condition shown in (56) represents a special case in which the effects of asymmetric depolarization are orthogonal to the aperture element polarization response.

One interpretation of (56) is that it may be possible, under certain scan conditions, for a linearly polarized aperture to have symmetric BSE, while a CP aperture, under the same scan conditions, has an asymmetric BSE. This is because $\hat{a}$ and $\hat{b}$ are purely directional unit vectors and have no phase difference. A linear aperture polarization may be orthogonal to either $\hat{a}$ or $\hat{b}$, but a CP aperture cannot be.

In general, (54) will not be satisfied, and BSE will be asymmetric. "Net symmetric" depolarization occurs only in BSE Region I, as explained in Section 2.5.1, and the case of aperture polarization orthogonality with the asymmetric depolarization

effect, as depicted in (56), occurs only under special scan conditions combined with certain element polarizations.

2.5.1 Net Depolarization Effect

Applying (49) to (27) allows a mathematical definition of "net depolarization". With arbitrary weighting of the rays and an approximation of constant transmission coefficients, a vector voltage sum from the monopulse processor may be represented as:

$$\begin{aligned}\sum \vec{E}^t &= \sum \ddot{T}\,\vec{E}^i \\ &= \left[T_{||} \begin{bmatrix} \sum_n A_n (\hat{a}\cdot\hat{u}_{||n})^2 & \sum_n A_n (\hat{a}\cdot\hat{u}_{||n})(\hat{b}\cdot\hat{u}_{||n}) \\ \sum_n A_n (\hat{a}\cdot\hat{u}_{||n})(\hat{b}\cdot\hat{u}_{||n}) & \sum_n A_n (\hat{b}\cdot\hat{u}_{||n})^2 \end{bmatrix} \right. \\ &\quad \left. + \; T_{\perp} \begin{bmatrix} \sum_n A_n (\hat{a}\cdot\hat{u}_{\perp n})^2 & \sum_n A_n (\hat{a}\cdot\hat{u}_{\perp n})(\hat{b}\cdot\hat{u}_{\perp n}) \\ \sum_n A_n (\hat{a}\cdot\hat{u}_{\perp n})(\hat{b}\cdot\hat{u}_{\perp n}) & \sum_n A_n (\hat{b}\cdot\hat{u}_{\perp n})^2 \end{bmatrix} \right] \vec{E}^i \end{aligned} \tag{57}$$

If a dielectric material other than air is assumed, and if:

$$\sum_n A_n (\hat{a}\cdot\hat{u}_{||n})(\hat{b}\cdot\hat{u}_{||n}) = 0 \quad \textit{and} \quad \sum_n A_n (\hat{a}\cdot\hat{u}_{\perp n})(\hat{b}\cdot\hat{u}_{\perp n}) = 0 \tag{58}$$

then (42) is satisfied in the summation of all rays incident on the aperture, and the "net depolarization" becomes "net symmetric":

$$\begin{bmatrix} \sum E_a^t \\ \sum E_b^t \end{bmatrix} = \left[T_{||} \begin{bmatrix} \sum_n A_n (\hat{a}\cdot\hat{u}_{||n})^2 & 0 \\ 0 & \sum_n A_n (\hat{b}\cdot\hat{u}_{||n})^2 \end{bmatrix} + T_{\perp} \begin{bmatrix} \cdots \\ \cdots \end{bmatrix} \right] \begin{bmatrix} E_a^i \\ E_b^i \end{bmatrix} \tag{59}$$

$$= \begin{bmatrix} \mathrm{T}_a & 0 \\ 0 & \mathrm{T}_b \end{bmatrix} \begin{bmatrix} E_a^i \\ E_b^i \end{bmatrix}$$

Due to the relationships between the unit vectors, both parts of (58) will simultaneously either be satisfied or not. However, in order for (58) to be identically satisfied, a certain relationship, such as defines BSE Region I, must exist between the surface normals within the aperture view.

Relationships between surface normals on an ogive radome, within an aperture view were determined to be either {(3) given (2)} or {(4) given (2)}, where in BSE Region I, all normals in the aperture view belonged to the set {(3) given (2)}, in Region III, all normals belonged to {(4) given (2)}, and in Region II, the normals were divided between the two sets. Examining Region I first, assuming quadrant symmetric weighting over N total elements, all rays may be divided into four sets, with a quadrant symmetric numbering scheme as indicated:

$$\sum_{n=1}^{N} A_n (\hat{a}\cdot\hat{u}_{||n})(\hat{b}\cdot\hat{u}_{||n}) = \sum_{i=1}^{N/4} A_i \left[(\hat{a}\cdot\hat{u}_{||i})(\hat{b}\cdot\hat{u}_{||i}) + (\hat{a}\cdot(-\hat{u}_{||i}))(\hat{b}\cdot\hat{u}_{||i}) + (\hat{a}\cdot\hat{u}_{||i})(\hat{b}\cdot(-\hat{u}_{||i})) + (\hat{a}\cdot(-\hat{u}_{||i}))(\hat{b}\cdot(-\hat{u}_{||i})) \right] \tag{60}$$

$$= 0$$

A similar expression may be written for the perpendicular case. Further, because an ogive is a figure of revolution, it can be determined from Figure 19 in BSE Region I:

$$\sum_n A_n (\hat{a}\cdot\hat{u}_{||n})^2 = \sum_n A_n (\hat{b}\cdot\hat{u}_{||n})^2 = \sum_n A_n (\hat{a}\cdot\hat{u}_{\perp n})^2 = \sum_n A_n (\hat{b}\cdot\hat{u}_{\perp n})^2 \qquad (61)$$

which means that the two remaining terms in the "net" transmission dyadic, T_a and T_b are equal. This means that both the net $\hat{a}$ and the net $\hat{b}$ components of the incident E-Field are acted upon equally by the radome. Applying (6) and (61) to (57) indicates that in BSE Region I, there will be no radome-induced BSE.

The other option for satisfying (54) is element polarization orthogonality to the asymmetric portion of the depolarization effect, described by (56). The two element monopulse processor can demonstrate a solution to the first half of (56). For a non-zero azimuth scan with L/R processing, the elements lie on the line defined by the intersection of the aperture plane and both the monopulse and scan planes. Given an element polarization $\hat{x}$, and $\hat{a}$ arbitrary, $\hat{a}$ may be chosen parallel to $\hat{x}$. At each of the two ray-radome intersection points, depolarization will be symmetric, i.e. $\alpha_{L1} = \alpha_{L2}$, $\beta_{L1} = \beta_{L2}$, $\alpha_{R1} = \alpha_{R2}$, and $\beta_{R1} = \beta_{R2}$. However, since the aperture is scanned out of BSE Region I, $\alpha_{L1} \neq \alpha_{R1}$ and $\beta_{L1} \neq \beta_{R1}$. Using these results in (54) gives:

$$Re\left\{ \frac{2(\beta_{L1} - \beta_{R1})\,\hat{b}\cdot\hat{p}_e}{2(\beta_{L1} + \beta_{R1})\,\hat{b}\cdot\hat{p}_e} \right\} \cong 0 \qquad (62)$$

which, in general, is zero only for $\hat{p}_e = \hat{x}$, given the orientation of $\hat{a}$. If the either the scan plane or the element polarization were changed, the BSE would be asymmetric.

2.5.2 Special Case: Hemispheric Radome

The hemisphere is a special case of an ogive with a length/width ratio of 1/2. If the aperture is gimballed at the center of the hemisphere, any scan angle, such that the aperture view does not reach the base of the radome, will satisfy the requirements for BSE Region I, as given in Section 2.1.2. On a general ogive, (60) and (61) are only satisfied when the aperture is in the unscanned position, but on a hemispheric radome, applying (60) and (61) predicts zero radome-induced BSE over an entire scan region.

3. Methodology

3.1 Model Validation and Use

Computer model results were compared to analytically predicted BSE behavior. The modeling technique used was originally developed by Temple; the technique was modified to simplify polarization sensitivity analysis, re-validated, and used to verify the predictions in Chapter 2. The model description is found in Section 3.2.1.

After model modifications had been made and revalidation completed, the model was applied to previously published results and experimental data. Input parameters, similar to the ones used by Burks [3] were input to the model. Differences between published parameters and ones used during the validation process are a result of modeling differences between the current model and Burks' model. Parametric differences are presented in Section 4.1. Results from the current model are nearly identical to those previously published, so the model was then applied to measured data. The agreement between predicted and measured BSE for a single polarization case, at two different frequencies, was the same as for Temple [1,6]. The comparison with measured data verified only that the modified model worked as well as the original.

Additionally, the model was applied to two empirical cases for which BSE could analytically be predicted to be zero. The predictions are in Sections 2.4.3 and 2.5.2, and the model results are mentioned in Section 4.4. As expected, modeled BSE results were zero at all scan angles, for both cases.

After validation, the model was applied to a production radar-radome system, but with various aperture polarizations and scan planes, creating the data shown in Section

4.3. For all cases considered, the model output results were consistent with the Chapter 2 predictions.

3.2 Model Description

3.2.1 Model Operation

The model is written in standard Fortran, and uses data files for program control and data input/output. The shell program reads the list of polarization states to be examined and performs the following tasks for each polarization state: 1) updates the system file, 2) calls a modified version of Temple's model as a subroutine, which calculates and reports BSE as a function of aperture scan location, and 3) stores the BSE results of each subroutine call in a file, indexed on the polarization state. The modifications are minor, mostly to allow the program to run as a subroutine and compile without all of its original options. Some minor improvements in execution efficiency were provided by Temple since his dissertation was completed.

The subroutine reads execution control variables, including scan angle range and updated polarization information, from the system input file. The radar and radome descriptions are also read from input files during subroutine execution. Using a modular input format such as this allows examination of multiple radar-radome combinations, with various scan options, using a simple file management scheme. A flow diagram is given in Figure 20.

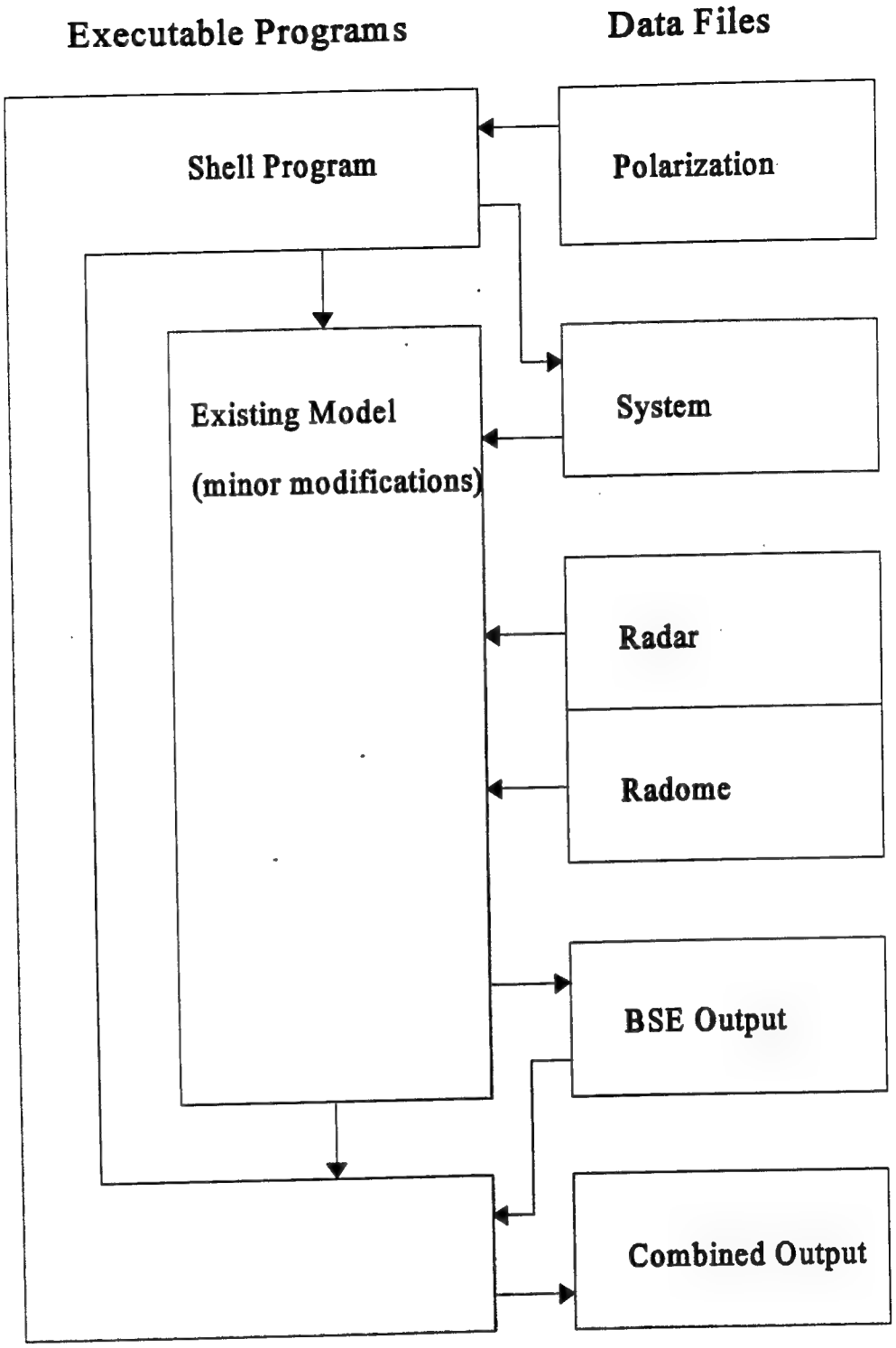

Figure 20 Model Flow Diagram

3.2.2 Model Theory

Aperture element voltages are calculated from incident E-Fields which have propagated via GO through the radome structure. Element voltages are combined, according to equations (5) and (6), to generate a monopulse error signal which represents an indicated source location angle relative to the aperture boresight. The difference between the indicated angle and the aperture scan angle is the radome-induced BSE.

Incident E-Fields are found using a GO ray-trace receive technique for direct rays. Each of the rays experiences amplitude, phase, and polarization distortion upon propagating through the radome. At each ray-radome intersection point a local plane of incidence is established and complex transmission coefficients calculated. The plane of incidence and these coefficients determine the effect of the radome structure on the rays. For a reference E-Field of strength E_r, with polarization orientation described by the unit vector $\hat{p}_r$ located a distance R from the n^{th} array element, the E-Field incident on the n^{th} array element is:

$$\vec{E}_e(n) = E_e(n)\,\vec{e}_e(n) \quad \textit{where} \quad \begin{cases} \vec{E}_r = E_r\,\hat{p}_r \\ E_e(n) = E_r\,e^{-jkR(n)} \\ \vec{e}_e(n) = T_{||}\left(\hat{p}_r \cdot \hat{u}^i_{||}\right)\hat{u}^t_{||} + T_{\perp}\left(\hat{p}_r \cdot \hat{u}^i_{\perp}\right)\hat{u}^t_{\perp} \end{cases} \tag{63}$$

where the parallel and perpendicular unit vectors are defined per Equation (15). The subscript e indicates the field at the element; r indicates the reference E-field; superscript i indicates the surface normal vectors on the incident side of the radome (outside); and

t indicates the transmitted side (inside) normals. Per Chapter 2 analysis, and the locally planar approximation, the inside and outside unit vectors are approximately parallel.

Multi-path reflected rays were not used in this analysis, although the model has the capability to include them. The model calculates multiple reflection points, angles, and coefficients. Reflected rays intersecting the front of the aperture combine to form total E-Fields incident on the elements. However, the improvement to model accuracy was negligible in contrast to the additional computation time.

The total incident E-Field, $\vec{E}^T(n)$ on the n^{th} array element is given by (64), where $\vec{E}_e^D(n)$ and $\vec{E}_e^R(n)$ are the incident E-Fields calculated for direct and reflected ray paths. The summation over m reflected E-Field terms accounts for multiple primary reflected ray paths for the n^{th} element. This is a model capability, although for this effort, the reflected fields were neglected and $\vec{E}^T(n)$ was set equal to $\vec{E}_e^D(n)$.

$$\begin{aligned} \vec{E}^T(n) &= \vec{E}_e^D(n) + \sum_{i=1}^{m} \vec{E}_e^R(n,i) \\ &= E^T(n)\,\vec{e}^T(n) \end{aligned} \tag{64}$$

The expression for the incident E-field in (63) reflects two important characteristics: the interaction between reference E-Field polarization and the surface normals, and accurate phase tracking. Since the original model already used the reference E-field polarization, it was well suited for a BSE polarization sensitivity analysis.

After finding the total E-field incident on an element, the model calculates the element's voltage response. Element polarization vectors $\hat{p}_e$ and $\hat{p}_h$ are used for CP and

XP field decomposition of $\vec{E}_e(n)$. The model requires all elements to have the same polarization response.

$$\begin{aligned}\vec{E}^T(n) &= E^T(n)\left\{\vec{e}^T(n)\cdot\hat{p}_e + \vec{e}^T(n)\cdot\hat{p}_h\right\} \\ &= \left\{\vec{E}_e^D(n)\cdot\hat{p}_e + \sum_{i=1}^{m}\vec{E}_e^R(n,i)\cdot\hat{p}_e\right\}\hat{p}_e \\ &\quad + \left\{\vec{E}_e^D(n)\cdot\hat{p}_h + \sum_{i=1}^{m}\vec{E}_e^R(n,i)\cdot\hat{p}_h\right\}\hat{p}_h \\ &= E_{CP}^T(n)\,\hat{p}_e + E_{XP}^T(n)\,\hat{p}_h\end{aligned} \tag{65}$$

The total voltage response, V_n, of each element is given by (66) where $E_{CP}^T(n)$ and $E_{XP}^T(n)$ are found by (65). The A_n and ϕ_n terms in (66) are amplitude and phase weights used to control pattern shape and main beam pointing direction. These are specified as model inputs for each element, allowing the model to use uniform, Taylor, or any other amplitude weighting scheme, and electronic scanning via phase control. As an approximation, the model assumes mutual coupling effects are identical for all elements within the array. For very large arrays with low sidelobe weighting, this approximation proves to be quite valid. As a result, the CP element pattern $f_e^{CP}(\theta,\phi)$, XP element pattern $f_e^{XP}(\theta,\phi)$, and element polarization directions $\hat{\rho}_e/\hat{\rho}_h$ are identical for all elements. Using independent CP and XP element patterns allows modeling multiple element types.

$$\begin{aligned}V_n &= A_n e^{j\phi_n}\left\{f_e^{CP}(\theta,\phi)\,E_{CP}^T(n) + f_e^{XP}(\theta,\phi)\,E_{XP}^T(n)\right\} \\ &= V_{CP}(n) + V_{XP}(n)\end{aligned} \tag{66}$$

Element voltages are calculated and summed in each of the symmetric quadrants shown in Figure 6. The quadrant sum voltages are then combined, as described in Section 2.1.3, equation (5), to form the appropriate monopulse sum and differences voltages, V_{SUM} and V_{DEL}, for either T/B or L/R BSE analysis. The monopulse error signal $E_{mp}(\hat{p},\gamma,\nu)$ is found from the complex monopulse voltage ratio V_{DEL}/V_{SUM}, over an angular range of γ for a $\hat{p}$ polarized incident wave at a frequency of ν. Monopulse sensitivity K is determined by the slope of the normalized difference pattern and has units of {(v/v)/Rad} [9].

$$E_{mp}(\hat{p},\gamma,\upsilon) = Re\left[\frac{V_{DEL}/V_{SUM}}{K}\right] = K^{-1}\frac{|V_{DEL}|}{|V_{SUM}|}\cos\left(\phi_{DEL} - \phi_{SUM}\right) \tag{67}$$

The monopulse error signal is used to establish system BSE, the angle indicated by (67) when the aperture scan direction equals the true source location. This is equivalent to fixing the aperture scan direction while repositioning the source until (67) equals zero. The angular difference between the scan direction and new source location is the system BSE. This is equivalent to the condition expressed in Equation (1).

4. Results and Discussion

Model results can be classified into two basic categories, either validation or prediction. Validation is a process whereby model results are compared with known or accepted results, i.e., empirical, published, and/or measured data. Validation is typically used to establish credibility for the particular modeling technique being employed. Once credibility is established, the modeling technique is used to produce results which extend beyond previously validated cases, usually by varying one or more variables/parameters of the system being modeled. The extended results for previously unvalidated cases are referred to as predictions. Provided system variables/parameters remain within prescribed limits or bounds, as dictated by assumptions made in developing the specific modeling technique, prediction results from the validated model are generally accepted as credible and form a basis for analyzing system performance.

Data presented in this chapter is provided in the order of investigation, with validation results preceding predictions. Empirical limiting case data, cases for which BSE equals zero for all polarizations and scan angles, is presented at the end of the chapter as a final validation step. For all of the cases examined, the coordinate system is fixed on the surface of the aperture, such that the reference E-Field polarization unit vectors, $\hat{a}$ and $\hat{b}$, and the aperture element polarization unit vectors, $\hat{x}$ and $\hat{y}$, always lie in the aperture plane. This arrangement dictates that the polarization plane of the reference E-Field is parallel to the aperture plane. For simplicity, $\hat{a}$ is chosen to be aligned with $\hat{x}$, which gives $\hat{b}$ as $-\hat{y}$. Scanning with the coordinate system fixed to the aperture surface is actually scanning the radome, but the relative positions are preserved.

4.1 Comparison with Published Data

For comparison with published results [3], data was generated using a uniform thickness (0.3166λ) tangent ogive radome. The radome is a single layer design of length 30.0λ, base diameter 10.0λ, and constructed of material with a relative dielectric constant of 3.2 and a loss-tangent of 0.008. The system is a mechanically scanned, 208-element circular aperture, approximately 8λ in diameter, with RCP polarized elements. The aperture is gimballed 2.0λ from the radome base and has a uniform amplitude.

The polarization cases used for obtaining previously published work are shown in Figure 21, along with the x-y coordinate system used to define the polarization tilt angle. Predicted BSE results are generated for two non-reflective I-Plane and X-Plane scanning cases, and are shown in Figures 22 through 25. Figures 22 and 23 represent the I-Plane scanning case and Figures 24 and 25 represent the X-Plane case. For both cases the aperture is scanned in the azimuth plane from 0° to 40° while the linearly polarized reference E-Field tilt angle is varied between ±90°. Current 2-D data (*,+,×) in Figures 23 and 25 represents specific polarization cases extracted from Figures 22 and 24, respectively, and is compared with the previously published results. In all cases, current BSE model results compare very well with the published results and clearly exhibit the polarization dependence identified previously [3]. Not evident in the 2-D comparisons, and hence not mentioned in previous work, is the asymmetric BSE characteristics in the 3-D plots of Figures 22 and 24. Given an arbitrary reference polarization, i.e., select a linearly polarized reference E-Field with an arbitrary tilt angle as the reference polarization state, any equal change (+ and -) in the polarization tilt angle about the reference angle results in an "asymmetric" BSE response.

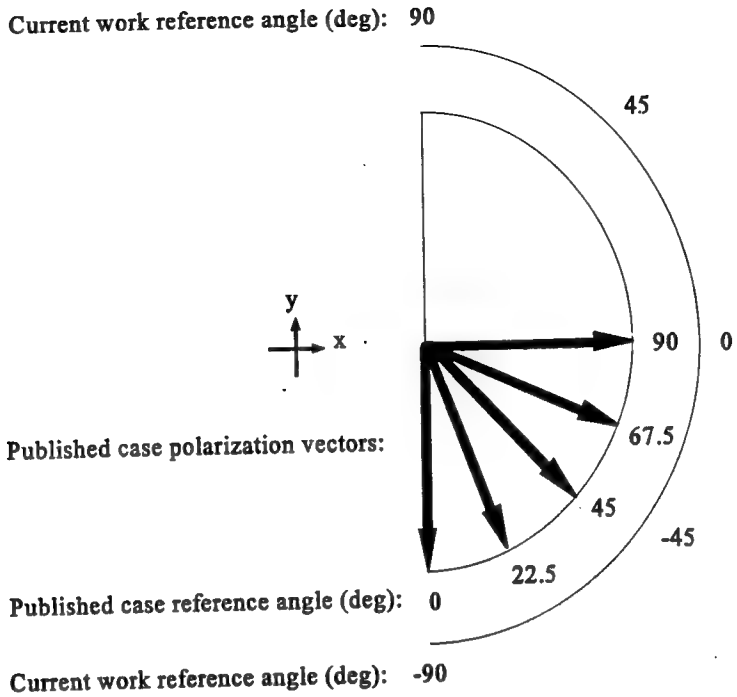

Figure 21 Published Case Polarization Vectors

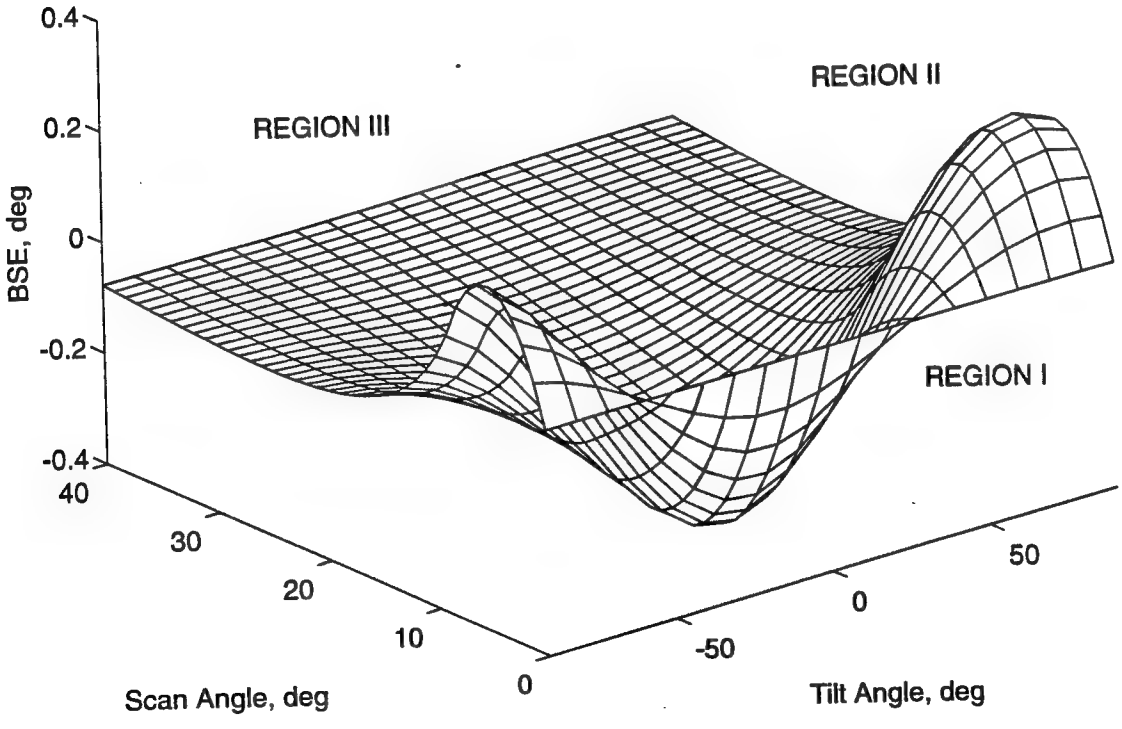

Figure 22 I-Plane BSE of Burks' Published Radar-Radome System

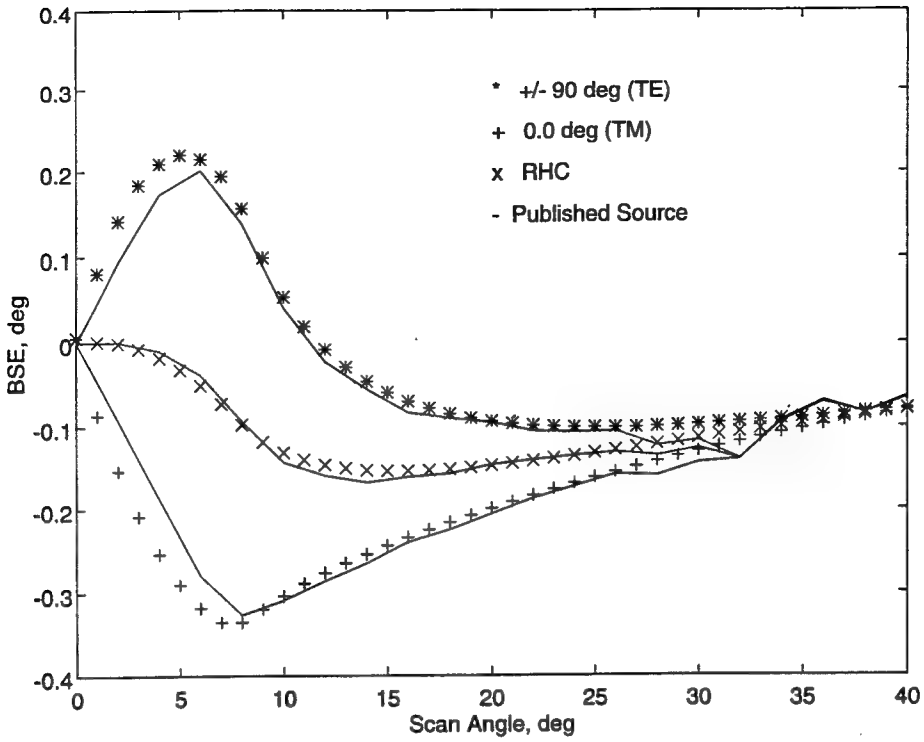

Figure 23 Comparison with Selected I-Plane Published Results

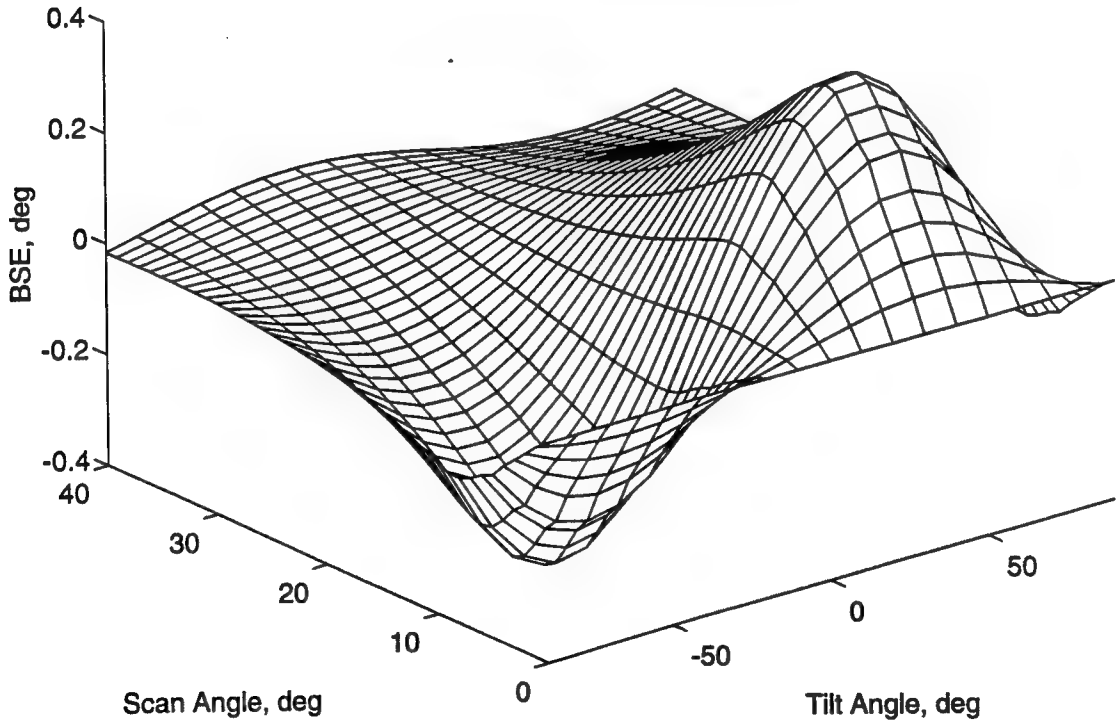

Figure 24 X-Plane BSE of Published Radar-Radome System

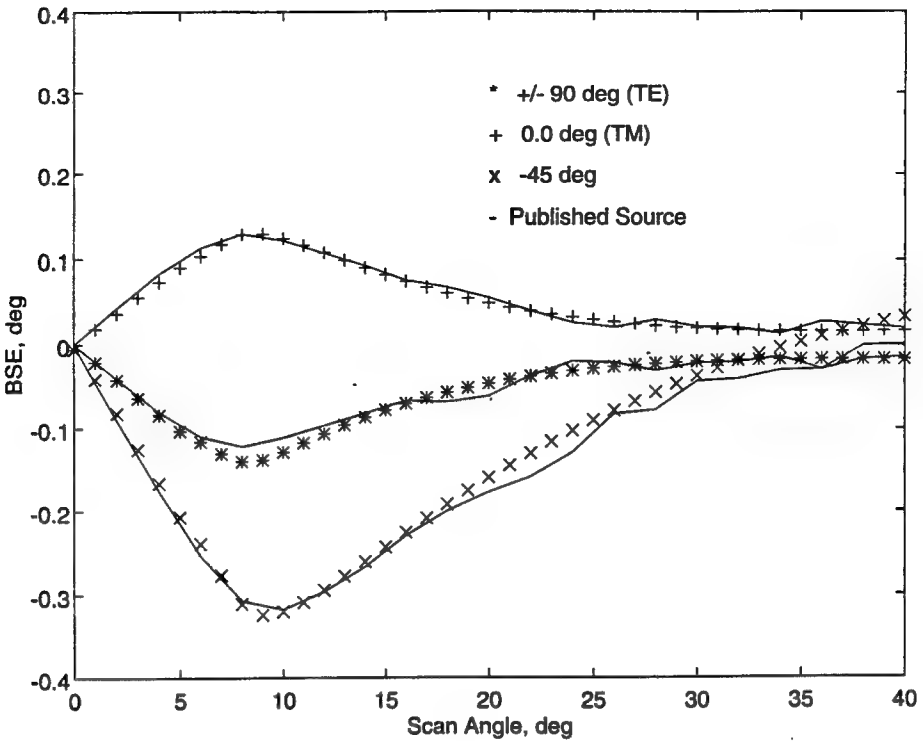

Figure 25 Comparison with Selected X-Plane Published Results

For example, select 0° as the reference polarization and compare the BSE values for the ±45° tilt angle cases in Figures 22 and 24. In general, at any given aperture scan angle, not only is +45° BSE is different than -45° BSE, but the relationship between +45° BSE and 0° BSE is "unrelated" to the relationship between 0° BSE and -45° BSE, i.e., it does not appear that any simple relationship exists for the different polarization cases.

4.2 Comparison with Measured Data

Model results are compared with measured BSE for a production radome, radar, and monopulse processing system. BSE values were averaged for three production radomes and model results were generated for input parameters based on production

system specifications. The production system is a mechanically scanned, 1368-element aperture, approximately 28-wavelengths in diameter with linearly polarized slotted waveguide elements. A modified cosine amplitude taper is applied across the aperture yielding a half-power beamwidth (HPBW) of approximately 2.488° and a first side-lobe level of approximately -30 dB. The radome is a solid tapered wall design empirically "tuned" to provide minimum BSE. It is modeled using a reference ogive surface with a length of 90.26λ, a base diameter of 36.136λ, and constructed of material with a nominal dielectric constant of 4.8 and a loss-tangent of 0.014. The aperture elements are linearly polarized and aligned in the $\hat{x}$ direction. The polarization tilt angle is measured relative to the aperture element polarization with a plus (+) sign indicating counterclockwise rotation and a minus (-) indicating clockwise rotation as viewed facing the aperture. Hence, for a tilt angle of 0° the reference E-Field and element polarization vectors are aligned. The polarization tilt angle is varied between ± 60° while the aperture scan angle is varied between 0° and 40°. Model results shown in Figure 26 are I-Plane BSE for the production system using a waterline scan (azimuth scan only, zero elevation) at the radome design frequency (FD). Figure 28 represents the same scan conditions using the higher frequency limit of the radome (FH). As predicted in Section 2.5.1, radome-induced BSE is independent of polarization tilt angle for the linear elements and the proper scan conditions. Figures 27 and 29 are extracted data from Figures 26 and 28, respectively, for the case where polarization tilt angle is zero. Measured data in the figures represents average BSE for three units randomly selected at the production facility. Comparison of measured BSE data with modeled results reveals a BSE prediction error of approximately 0.028° (0.5 mRad), identical to previous results [1, 6].

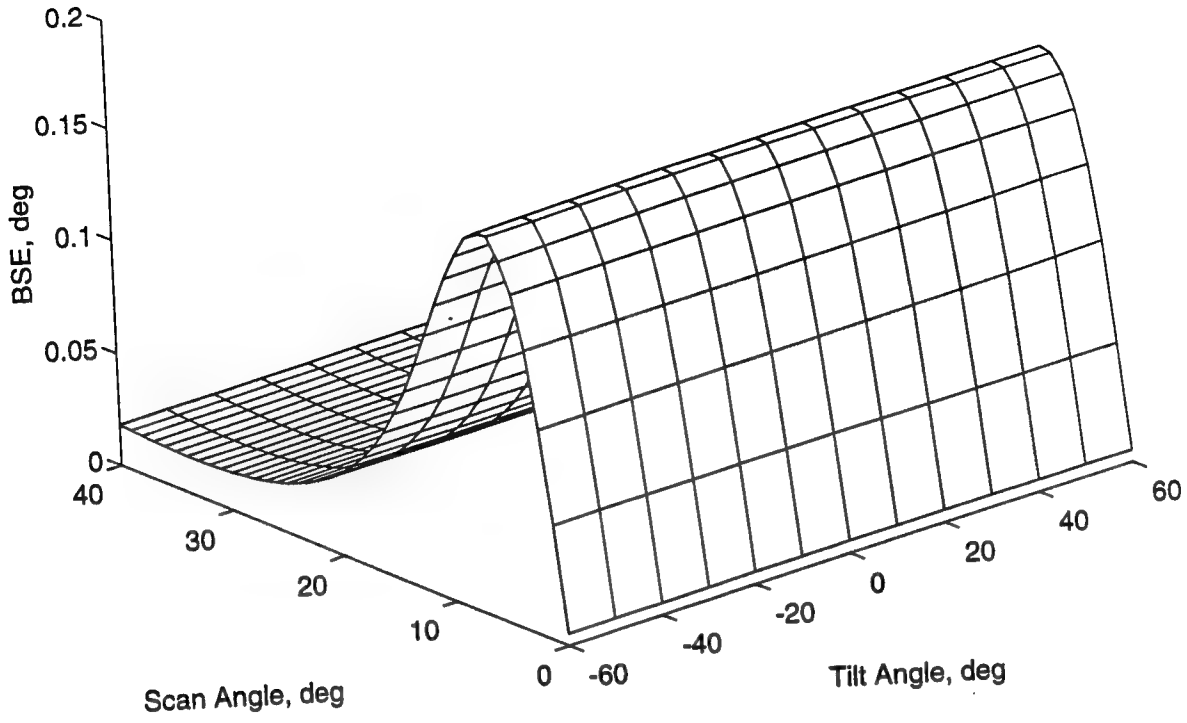

Figure 26 I-Plane BSE of Production System, Azimuth Scan, FD

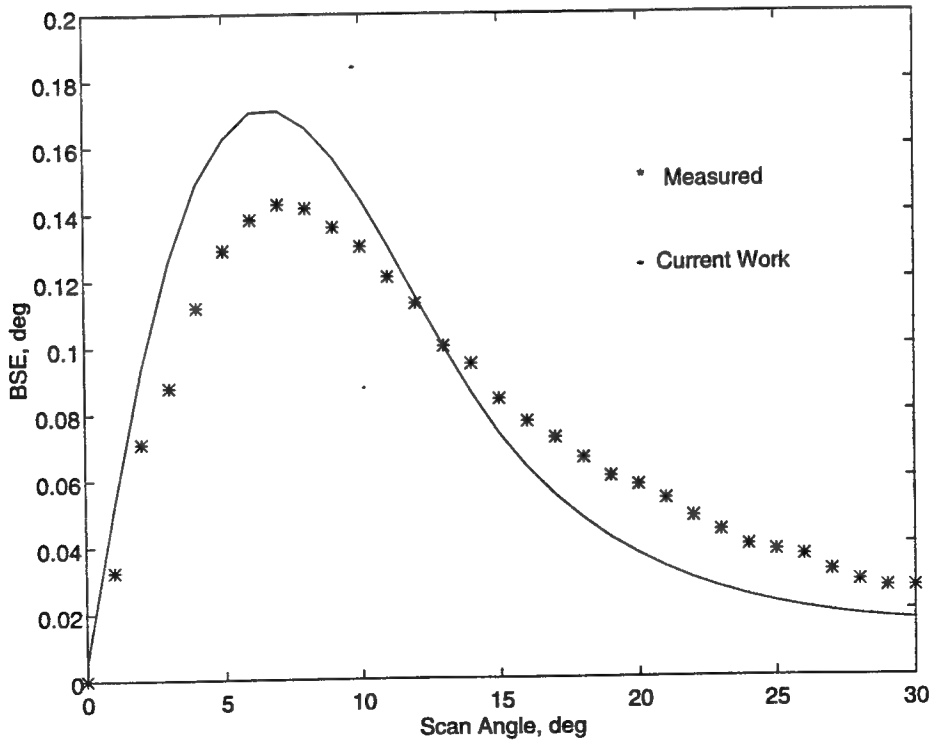

Figure 27 Comparison with Measured I-Plane Results, FD

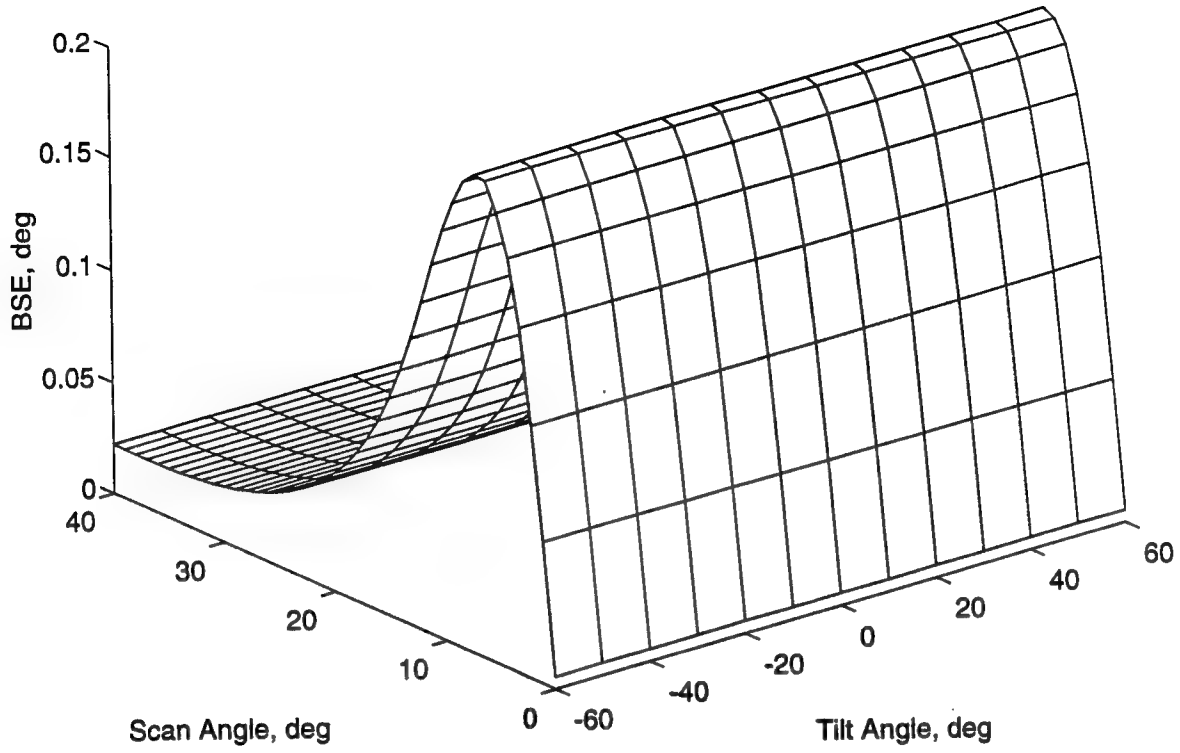

Figure 28 I-Plane BSE of Production System, Azimuth Scan, FH

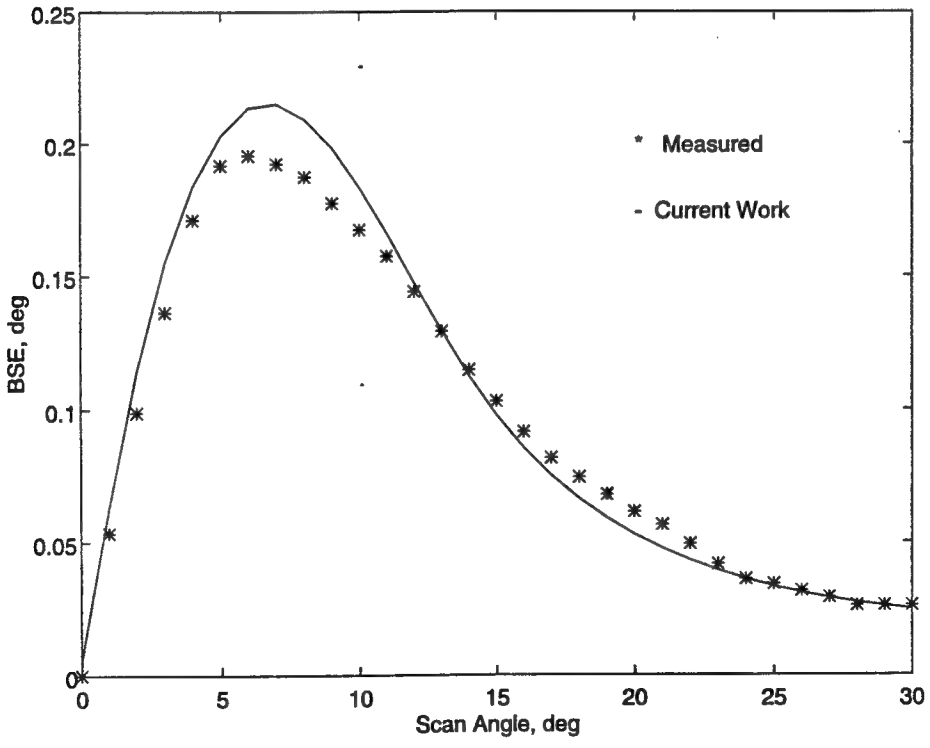

Figure 29 Comparison with Measured I-Plane Results, FH

4.3 Model Results of Asymmetric BSE

To examine the asymmetric behavior of radome-induced BSE using various polarizations, model results are generated using the production system with a diagonal aperture scan and $\hat{x}$ elements, and a waterline scan with CP elements. Figure 30 is the I-Plane BSE (azimuth BSE) for the production system using a diagonal scan (45° azimuth-elevation plane). Figures 31 and 32 are I-Plane BSE results for waterline and diagonal scans at FD, respectively.

In all cases, BSE exhibits the asymmetric polarization dependence predicted in Section 2.5. Four variables affecting BSE for a given radar-radome system are 1) scan angle, 2) scan plane, 3) frequency, and 4) reference E-Field polarization. But, fixing these four variables, BSE can be expressed and analyzed as a function of aperture element polarization. Noting that the simple superposition of RCP and LCP E-Fields produces a scaled LP E-Field,

$$(\hat{x} + j\hat{y}) + (\hat{x} - j\hat{y}) = 2\hat{x} \tag{68}$$

we obtain the question of whether the BSE of RCP, LCP, and LP apertures are related. Specifically, performing a point-by-point addition of BSE values, indexed on polarization tilt angle and scan angle, and allowing for an arbitrary scale factor, α, is:

$$[BSE(LCP) + BSE(RCP)] \triangleq \alpha\, BSE(LP) \tag{69}$$

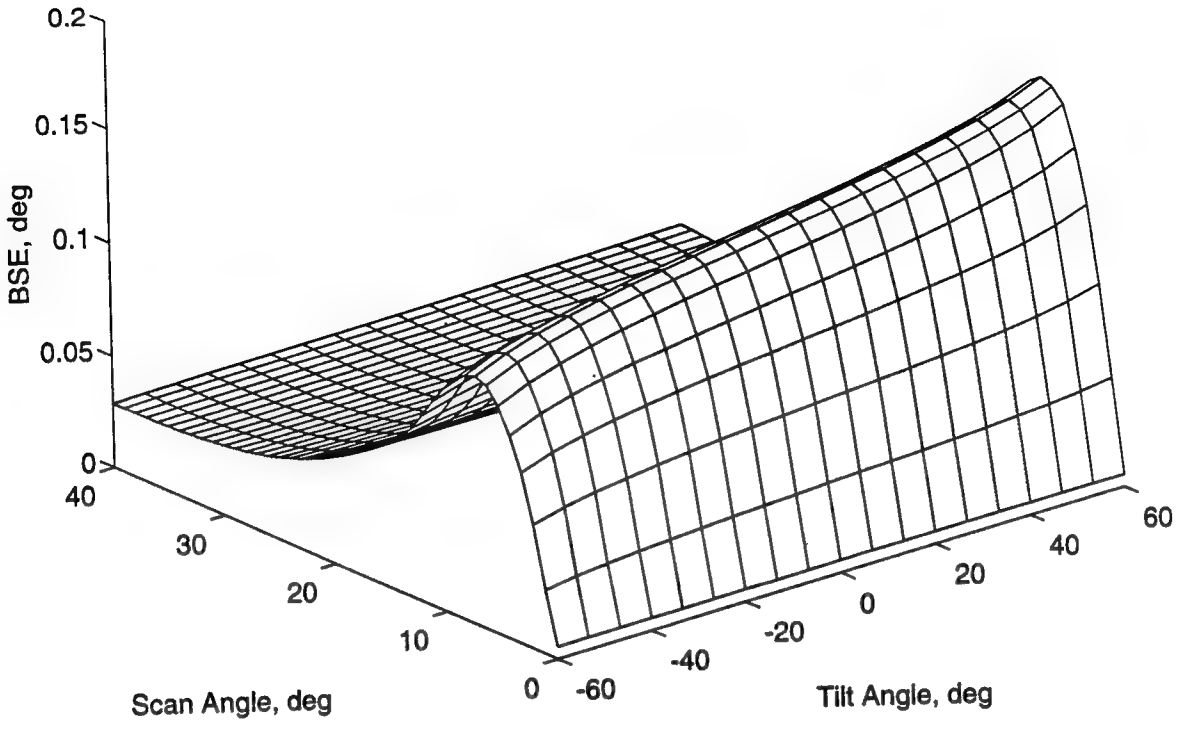

Figure 30 I-Plane BSE of Production System, Diagonal Scan, FD

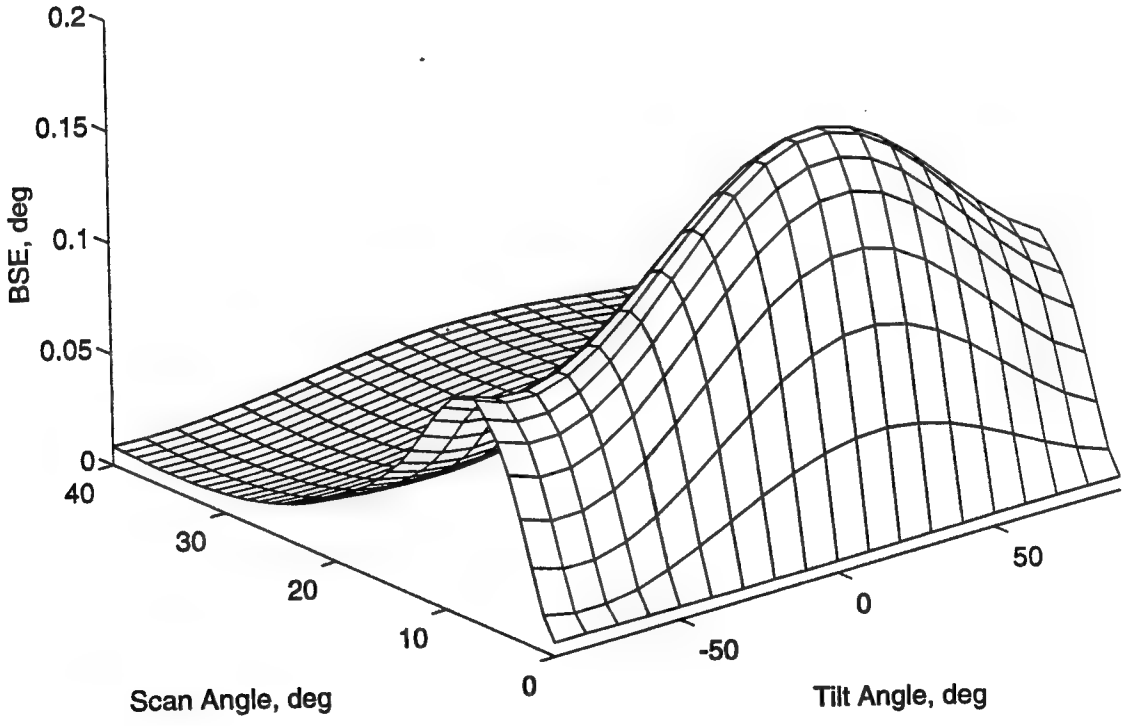

Figure 31 I-Plane BSE of Production Radome, RCP Aperture, Azimuth Scan, FD

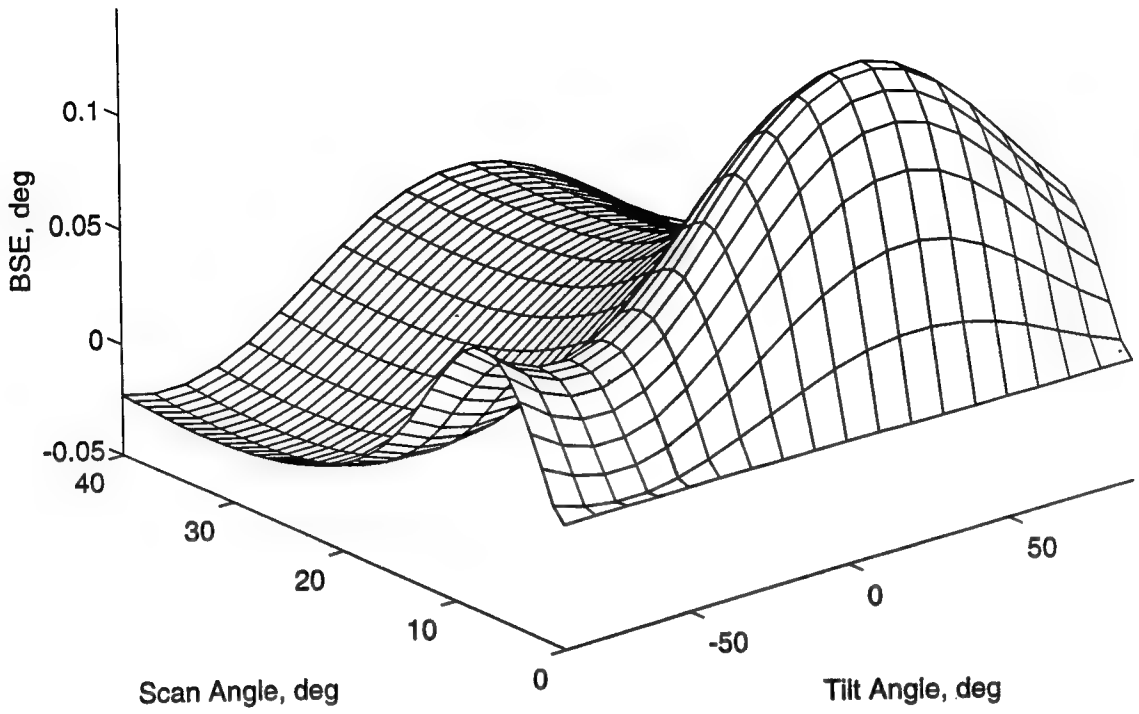

Figure 32 I-Plane BSE of Production Radome, RCP Aperture, Diagonal Scan, FD

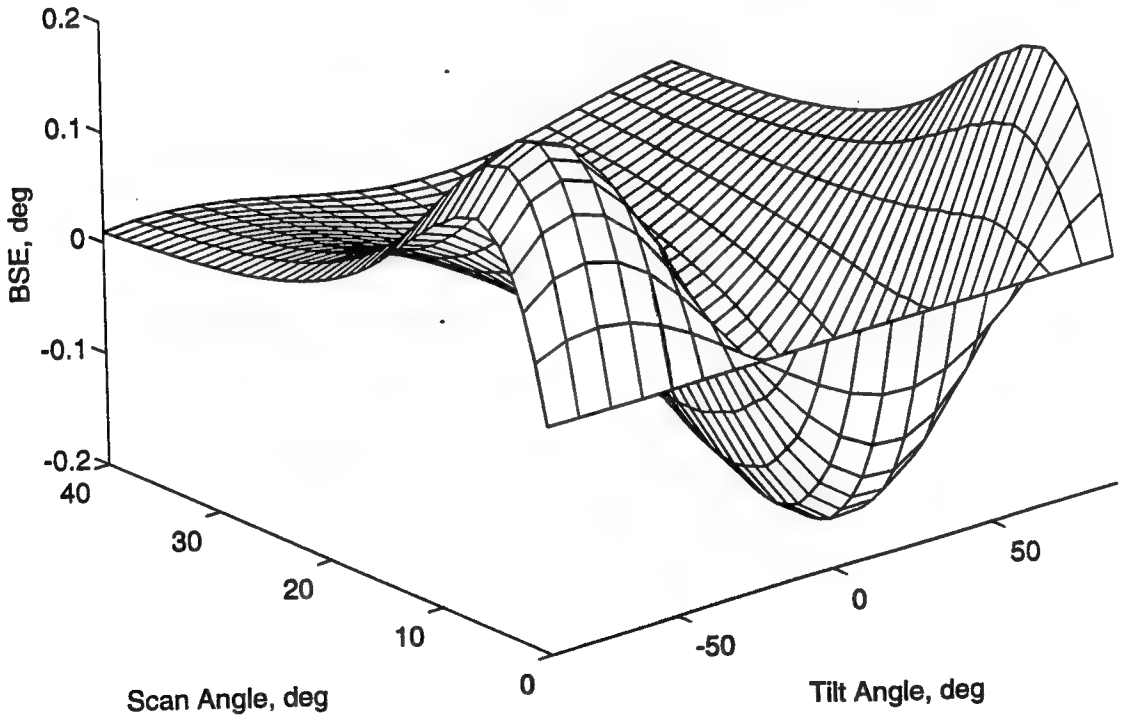

Figure 33 I-Plane BSE of Production Radome, LCP Aperture, Azimuth Scan, FD

However, examination of Figure 33 shows that this is not the case. Point-by-point addition of Figures 31 and 33 does not produce a scaled version of Figure 26, indicating that BSE is a non-linear function of polarization. This somewhat surprising result can be explained by using a simplified version of (51) in (69), where A and B represent the vector difference and sum voltages, respectively:

$$\frac{1}{2}\left[\frac{\vec{A}\cdot(\hat{x}-j\hat{y})}{\vec{B}\cdot(\hat{x}-j\hat{y})}+\frac{\vec{A}\cdot(\hat{x}+j\hat{y})}{\vec{B}\cdot(\hat{x}+j\hat{y})}\right]\triangleq\frac{\vec{A}\cdot\hat{x}}{\vec{B}\cdot\hat{x}} \tag{70}$$

which is true only if:

$$\vec{A}\cdot(\hat{x}-j\hat{y})\vec{B}\cdot(\hat{x}+j\hat{y})\vec{B}\cdot\hat{x}+\vec{A}\cdot(\hat{x}+j\hat{y})\vec{B}\cdot(\hat{x}-j\hat{y})\vec{B}\cdot\hat{x}\triangleq 2\vec{A}\cdot\hat{x}\vec{B}\cdot(\hat{x}-j\hat{y})\vec{B}\cdot(\hat{x}+j\hat{y}) \tag{71}$$

Expanding gives:

$$(A_x-jA_y)(B_x+jB_y)(B_x)+(A_x+jA_y)(B_x-jB_y)(B_x)\triangleq 2(A_x)(B_x-jB_y)(B_x+jB_y) \tag{72}$$

Finally, in general:

$$2A_xB_x^2+2A_yB_xB_y\neq 2A_xB_x^2+2A_xB_y^2 \tag{73}$$

indicating that for any α:

$$[BSE(LCP)+BSE(RCP)]\neq\alpha\,BSE(\hat{x}) \tag{74}$$

Superposition of element polarizations is not applicable to determine BSE. For example, one cannot easily deduce BSE behavior for an LCP aperture, given BSE behavior for RCP and LP apertures.

4.4 Empirical Cases

Final model validation included two empirical limiting cases for which radome-induced BSE is known to be zero, not only by the methods in Sections 2.4 and 2.5, but also by intuition. In both cases, the model correctly predicted no BSE.

4.4.1 Air Radome

The model was run using a radome of the same dimensions as the production radome, but with no loss tangent and a relative permittivity and permeability of 1.0. This is equivalent to an "air" production radome, which is essentially no radome at all. The aperture arm length and gimbal point were the same as the production system. In Section 2.4.3, the transmission dyadic reduced to an identity matrix and the analysis predicted no radome-induced depolarization, and hence no radome-induced BSE. Model results correctly indicate no BSE for any combination of reference E-Field polarization and scan angle.

4.4.2 Hemispheric Radome

The model was run using a hemispheric radome with the same relative permittivity and permeability as the production radome, but with no loss tangent. The aperture arm length was set to 0.0 and gimbal point was placed at the center of the hemisphere. Per

Section 2.1.2, this results in the entire scan region being defined as BSE Region I. The net transmission dyadic of Section 2.4.3 becomes symmetric, and analysis predicts no net radome-induced depolarization, and hence no radome-induced BSE. Model results correctly indicate no BSE for any combination of reference E-Field polarization and scan angle.

5. Conclusions and Recommendations

A polarization dependent GO propagation technique is extended to analyze and model electrically large radome-radar monopulse processing systems. Extended model results are validated against empirical, published experimental, and measured BSE data for a production radome-radar system. Radome-induced BSE is characterized under varying polarization conditions, i.e., reference E-Field versus element polarization and scan angle, and found to exhibit a considerable amount of dependence/sensitivity for specific cases considered. Generally, BSE exhibits dependence on both aperture scan angle and reference E-Field polarization. Only in special cases of either linearly polarized apertures, or specifically constructed radomes, is BSE relatively insensitive to polarization variations of the reference E-Field.

The dependence of BSE on both aperture scan angle and incident polarization could greatly complicate the simplest table look-up scheme for BSE calibration or even have a major impact on the overall monopulse system design. Although aperture scan angle is generally available, from either electrical or mechanical positioning components, monopulse systems do not typically "measure" or estimate incident wave polarization; such systems, as currently designed, are therefore incapable of correctly calibrating out or correcting for radome-induced BSE resulting from polarization variations.

Areas for extending the current work include analyzing BSE polarization sensitivity for electronically scanned apertures, modeling frequency selective surface (FSS) radomes, including reflected ray conditions, optimizing the model to reduce

execution time. Electronically scanned apertures may exhibit slightly different BSE behavior with scan position due to the shrinkage of the "effective aperture" with increasing scan angle off-boresight. Also, a greater number of reflected rays will intercept the face of an electronically scanned aperture when compared to the mechanically scanned case, influencing BSE at higher scan angles. In all likelihood, the general shape of the BSE curve as a function of both scan angle and polarization should be similar to the mechanically scanned aperture.

Reflected rays affect BSE at higher scan angles (greater than 25° for the radar-radome systems considered under this effort), and a reflected ray analysis should include development of a reflection dyadic expression equivalent to the transmission dyadic. Including reflected rays in the analysis and modeling would increase BSE prediction accuracy at higher scan angles. Reflected E-Field depolarization effects may also exhibit additional asymmetric properties when compared to transmission depolarization. Also, the present transmission dyadic is applicable only to thin, non-FSS radomes. An extension to a FSS dyadic would include TE to TM and TM to TE coupling effects.

Although the model provides accurate results, many redundant operations resulted from calling the original model as a subroutine. Excellent potential exists for reducing execution time, by simply moving certain portions of the original model into a new shell program. The code is modular, which facilitates the reprogramming task. If the model were to be used for an actual engineering effort, optimization would be worthwhile.

Bibliography

[1] Temple, Michael A., *Radome Depolarization Effects on Monopulse Receiver Tracking Performance*, Dissertation, Air Force Institute of Technology AFIT/DS/ENG/93-03, June 1993.

[2] Sherman, Samuel M., *Monopulse Principles and Techniques.* Massachusetts: Artech House, 1984.

[3] Burks, D.G., E.R. Graf, and M.D. Fahey, "A High Frequency Analysis of Radome-Induced Radar Pointing Error," *IEEE Trans. Antennas Propagat.*, **AP-30**, Sep '82, pp. 947-955.

[4] Huddleston, G.K., H.L. Bassett, and J.M. Newton, "Parametric Investigation of Radome Analysis Results: Salient Results," Vol I of IV, Technical Report, AFOSR-77-3469, Bolling AFB, 1981.

[5] Klemer, D.P., "Effects of Refraction by an Ogive Radome on Radome Boresight Error," Technical Report #675, Lincoln Laboratory, Massachusetts Institute of Technology, 1984.

[6] Temple, Michael A., *Radome Depolarization and Phase Front Distortion Effects on Boresight Error Prediction*, IEEE Aerospace and Electronic Systems Society, National Radar Conference, 1994.

[7] Kraus, John D., *Electromagnetics, Fourth Edition.* New York: McGraw-Hill, 1992

[8] Munk, B.A., G.A. Burrell, and T.W. Kornbau, "General Theory of Periodic Surfaces in a Stratified Medium," Technical Report, AFAL-TR-77-219, The Ohio State University, 1977.

[9] Siwiak, K., T.B. Dowling and L.R. Lewis, "Boresight Errors Induced by Missile Radomes," *IEEE Trans. Antennas Propagat.*, **AP-27**, Nov '79, pp. 832-841.

REPORT DOCUMENTATION PAGE

Form Approved
OMB No. 0704-0188

1. AGENCY USE ONLY (Leave blank)	2. REPORT DATE	3. REPORT TYPE AND DATES COVERED
	December 1994	Master's Thesis

4. TITLE AND SUBTITLE
POLARIZATION SENSITIVITY OF MONOPULSE RADAR BORESIGHT ERROR INDUCED BY LARGE, OGIVE RADOMES

5. FUNDING NUMBERS

6. AUTHOR(S)
Kelce S. Wilson, Capt, USAF

7. PERFORMING ORGANIZATION NAME(S) AND ADDRESS(ES)
Air Force Institute of Technology, WPAFB OH 45433-6583

8. PERFORMING ORGANIZATION REPORT NUMBER

9. SPONSORING/MONITORING AGENCY NAME(S) AND ADDRESS(ES)
Mike Temple, Capt, USAF
Wright Laboratory, AAWD-1
WPAFB, OH 45433-6534

10. SPONSORING/MONITORING AGENCY REPORT NUMBER

11. SUPPLEMENTARY NOTES

12a. DISTRIBUTION/AVAILABILITY STATEMENT
Approved for public release; distribution unlimited

12b. DISTRIBUTION CODE

13. ABSTRACT *(Maximum 200 words)*

The dependence of Boresight Error (BSE) on incident Electric Field (E-Field) polarization tilt angle is investigated. BSE, defined as the angular difference between a target's actual and radar-indicated position, is influenced by the radome used to protect the antenna. A reliable computer model for predicting the BSE of electrically large radar-radome systems has been demonstrated and used to investigate the dependence of radome-induced BSE for various combinations of scan angle, element polarization, and incident E-Field polarization. The analysis includes a development of a transmission/depolarization model to justify the results of the computer model. Results compare very well with empirical, published, and experimentally measured data for specific scan angle and polarization cases considered. Generally, BSE exhibits a noticeable dependence on E-Field polarization, except under limited scanning conditions for specific linearly polarized antenna apertures.

14. SUBJECT TERMS	15. NUMBER OF PAGES
Boresight Error, Monopulse Radar, Ogive, Polarization Radome	90
	16. PRICE CODE

17. SECURITY CLASSIFICATION OF REPORT	18. SECURITY CLASSIFICATION OF THIS PAGE	19. SECURITY CLASSIFICATION OF ABSTRACT	20. LIMITATION OF ABSTRACT
Unclassified	Unclassified	Unclassified	UL